INFLUENCE OF HYDROGEN ANNEALING AND SUBSTRATE TEMPERATURE ON THE PROPERTIES OF RF SPUTTERED ZINC OXIDE THIN FILMS

BY

ALADE IBRAHIM OLANREWAJU

A Thesis Presented to the

DEANSHIP OF GRADUATE STUDIES

KING FAHD UNIVERSITY OF PETROLEUM & MINERALS

DHAHRAN, SAUDI ARABIA

In Partial Fulfillment of the
Requirements for the Degree of

MASTER OF SCIENCE

In

PHYSICS

DECEMBER 2014

KING FAHD UNIVERSITY OF PETROLEUM & MINERALS

DHAHRAN- 31261, SAUDI ARABIA

DEANSHIP OF GRADUATE STUDIES

This thesis, written by Alade Ibrahim Olanrewaju under the direction of his thesis advisor and approved by his thesis committee, has been presented and accepted by the Dean of Graduate Studies, in partial fulfillment of the requirements for the degree of MASTER OF SCIENCE IN PHYSICS.

Department Chairman

Dr. Abdullah A. Al-Sunaidi

12.1.2015

Advisor

Prof. Mohammad F. Al-Kuhaili

Co-advisor

Prof. Sardar Mohammed Ayub Durrani

Dean of Graduate Studies

Dr. Salam A. Zummo

Member

Dr. Fatah. Z. Khiari

12/1/15

Date

Member

Dr. Mohammad Baseer Haider

Member

Dr. Saleem Rao

DEDICATION

This whole work is dedicated to my loving late mother, Mrs Alade Felicia Abiodun

ACKNOWLEDGMENTS

I am highly indebted to my supervisor Dr. Mohammed Al-Kuhaili for his insight and moral support during the entire period of this work. Without his guidance, this work would have suffered many setbacks. He made painstaking efforts in correcting the manuscript. His exceptional professionalism and high ethical values are lessons that would remain indelible in my memory.

My special thanks go to members of my committee- Dr. Ayub, Dr. Khiari, Dr. Haider and Dr. Rao. I really appreciate all their input in this work.

I am equally very grateful to all faculty members in physics for their friendly attitude towards me during my stay at KFUPM regarding my academic studies and research, especially those with whom I took courses. Their efforts really transformed my perception of physics and have made studying physics more of a hobby than anything else.

The generous scholarship that I received from King Fahd University Petroleum and Minerals (KFUPM) is the key to the successful completion of my master's program in physics. I am highly honored to have been awarded this scholarship.

There are many people behind the scene whose support is very critical to my academic stability. Notable among them is my late mother, father, wife and other members of my family. They sacrificed their right upon me. If not for their understanding and prayers, it would have been difficult to complete my M.Sc program successfully. I am very grateful for all of their support.

To Allah definitely belongs all the praise and adoration. Finally, which of the favors of my lord will I deny? None. Alihamdullahi Robil alamin

TABLE OF CONTENTS

LIST OF TABLES

LIST OF FIGURES

LIST OF ABBREVIATIONS

AFM: Atomic force microscopy.

B.E: Binding Energy.

F1-As : As deposited films without substrate heating.

F1-300: Films deposited on unheated substrates and annealed at 300 ^{o}C.

F1-400: Films deposited on unheated substrates and annealed at 400 ^{o}C.

F2-As: As deposited films with substrate heating.

F2-300: Films deposited on heated substrates and annealed at 300 ^{o}C.

F2-400: Films deposited on heated substrates and annealed at 400 ^{o}C.

FWHM: Full width at half maximum.

HBE: High binding energy.

IME: Intermediate binding energy.

LBE: Low binding energy.

XRD: X-ray diffraction.

XPS: X-ray photoelectrons spectroscopy.

ABSTRACT

Full Name : Alade Ibrahim Olanrewaju.

Thesis Title : The Influence of hydrogen annealing and substrate temperature on the properties of RF sputtered zinc oxide thin films.

Major Field : Physics.

Date of Degree: December, 2014.

Zinc oxide (ZnO) is an important material that has been investigated for several technological applications, such as ultraviolet optoelectronics, transparent conductors, photovoltaics and gas sensing. ZnO is characterized by its excellent attributes, such as a wide band gap (3.3 eV) and a high exciton binding energy. For ZnO to be adopted for these applications, its properties have to be suitably modified to meet certain requirements. In this work, the influence of hydrogen annealing and substrate temperature on the properties of radio-frequency (RF) sputtered zinc oxide thin films were studied. First, the effect of hydrogen annealing temperature on the properties of zinc oxide films deposited on unheated substrates was studied. The range of temperatures under investigation was 300 to 600 ^{o}C in steps of 100 ^{o}C. Second, the effect of substrate heating was also investigated at 400 ^{o}C. Structural properties of the films were characterized using X-ray diffraction (XRD) and atomic force microscopy (AFM)

techniques. Chemical analysis was done with the aid of X-ray photoelectron spectroscopy (XPS). The optical and electrical properties were studied using spectrophotometry and and Hall measurement techniques, respectively. The films were all polycrystalline with (002) orientation as the most preferred growth direction for films deposited on unheated substrates. However, this direction was altered to (100) by substrate heating. Furthermore, the films showed improvement in the lateral grain size and crystallinity upon annealing. The chemical analysis revealed the increase in oxygen vacancies upon annealing. The electrical results revealed that the highest conductivity was obtained when the films were deposited on heated substrates and annealed at 400 ^{o}C. Reduction in the resistivity of the annealed films was attributed to increased oxygen vacancies, while desorption of oxygen at the grain boundary was responsible for the increased mobility. There was a slight reduction or increase in the band gap for films deposited on unheated or heated substrate, respectively. The increase in the band gap was attributed to Burstein-Moss effect.

ملخص الرسالة

الاسم الكامل:ألادي إبراهيم أولانريواجو

عنوان الرسالة:تأثير التسخين الهيدروجيني ودرجة حرارة الركيزة على خصائص أغشية أوكسيد الزنك الرقيقة

التخصص:: فيزياء

تاريخ الدرجة العلمية:ديسمبر 2014م

أكسيد الزنك (أكسيد الزنك) مادة هامة يتم دراستها من أجل عدة تطبيقات تكنولوجية، مثل الإلكترونيات الضوئية فوق البنفسجية، الموصلات الشفافة، وحدات الطاقة الشمسية، والكشف عن الغازات. يتميز أكسيد الزنك بخصائص ممتازة، مثل وجود فجوة واسعة النطاق (3.3 ألكترون فولت) وطاقة ربط عالية للإكسيتون. ولأجل استخدام أكسيد الزنك في هذه التطبيقات، فإن خصائصه لا بد من تعديلها بشكل مناسب لتلبية متطلبات معينة. في هذا البحث، سندرس تأثير التلدين الهيدروجيني ودرجة حرارة الركيزة على خصائص أغشية أكسيد الزنك. أولا، تم دراسة تأثير درجة حرارة التلدين الهيدروجيني على خصائص أغشية أكسيد الزنك المترسبة على ركائز غير مسخنة. وكان نطاق درجات الحرارة في هذا البحث من 300 إلى 600 درجة مئوية بخطوات 100 درجة مئوية. ثانيا، تم دراسة تأثير تسخين الركيزة أيضا عند 400 درجة مئوية. ودرسنا الخصائص الهيكلية للأغشية باستخدام حيود الأشعة السينية (XRD) ومجهر القوة الذرية(AFM) . وقد تم التحليل الكيميائي بمساعدة طيف الأشعة السينية الضوئية XPS. تم دراسة الخصائص البصرية والكهربائية باستخدام تقنيات القياس الطيفي

الضوئي وقياسات هول، على التوالي. وكانت الأغشية كلها متعددة البلورات والتوجه (002) هو اتجاه النمو الأكثر تفضيلا للأغشية الناشئة على ركائز غير مسخنة. ومع ذلك، تم تغيير هذا الاتجاه إلى (100) عن طريق تسخين الركيزة. وعلاوة على ذلك، أظهرت الأغشية تحسناً في حجم الحبيبات والتبلور مع التسخين. وكشف التحليل الكيميائي زيادة في شواغر الأكسجين مع التسخين. وكشفت النتائج الكهربية أن أعلى موصلية تم الحصول عليها عندما ترسبت الأغشية على ركيزة ساخنة، وتسخينها إلى 400 درجة مئوية. ويعزى النقص في مقاومة الأغشية المسخنة إلى زيادة عدد شواغر الأوكسجين. وتعزى زيادة الأكسجين في الحدود بين الحبيبات إلى زيادة التحريك. ولوحظانخفاض طفيف، وزيادة الفجوة للأغشية المترسبة على ركيزة غير مسخنة وركيزة ساخنة، على التوالي. ويعزى زيادة الفجوة إلى تأثير بورستين موس.

CHAPTER ONE

INTRODUCTION

Zinc oxide is one of the most useful technological materials because it possesses a number of excellent properties such as electro-optical, semiconducting, piezoelectric, acoustic-optical and photo-conductive properties [1, 2]. The interest in zinc oxide started several decades ago. The reason for this is because zinc oxide is utilized in many industries, such as chemical, rubber, ceramics, agricultural, pharmaceutical and semiconductor [3] .

Recently, the interest in zinc oxide is centered on potential semiconductor and electronics applications. The reasons behind ZnO receiving a considerable amount of research in these fields is due to its large direct band gap of approximately 3.3 eV, high exciton binding energy of 60 meV, and high thermal and mechanical stability at room temperature [4-7]. Also, it can be prepared with reproducible results through various techniques such as vacuum evaporation [8] , spray pyrolysis [9] and sputtering [10] .

Transparent conducting oxide (TCO) films is another research area that is presently of huge commercial and scientific significance for applications in flat panel displays, electro chromic windows, electro-optical devices, and solar cells [10,11]. Zinc oxide has been a viable candidate in this field, owning to its abundance in nature, low cost, non-toxicity, and stability in hydrogen plasma processes [5,12,13]

Because of the role played by crystal and defect structures on the optical, electrical and structural properties of zinc oxide, I shall briefly discuss the basic properties of ZnO and the associated defects. Then, the scope of this thesis will be presented.

1.1 Properties of Zinc Oxide

In the periodic table, zinc and oxygen belong to group II &VI, respectively. Zinc has two valence electrons, while oxygen has six valence electrons. These two elements combine chemically to form an ionic compound. It has been observed that the group II –VI binary compounds crystallize in either hexagonal wurtzite or cubic zinc blende structures. In either of the two structures, each zinc ion is surrounded by four oxygen ions at the edges of tetrahedrons. This tetrahedral arrangement is common with the sp^3 covalent bonding. Hence, zinc oxide has an ionicity that lies between ionic and covalent bonding. The presence of ionic bonding in ZnO accounts for the wide band gap energy [14]. Figure 1.1 below gives a schematic representation of the various forms of the ZnO crystal structures.

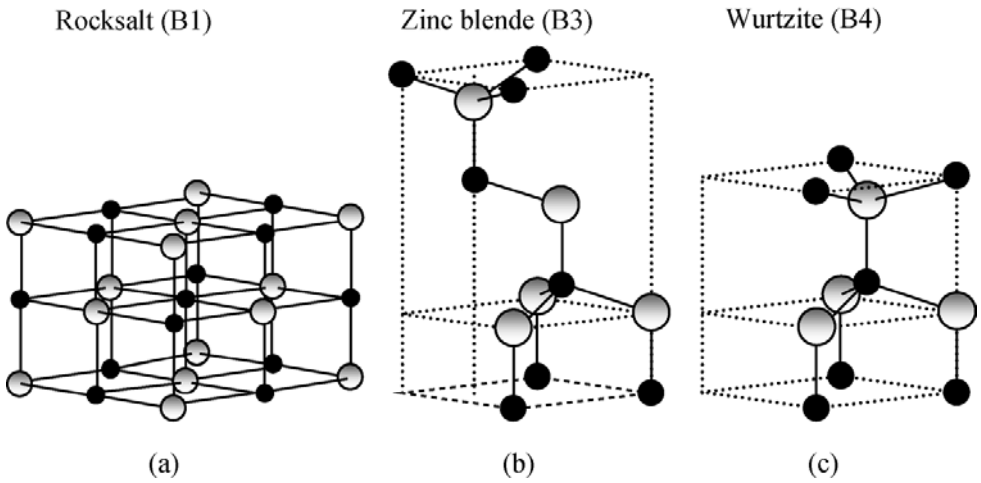

Figure 1.1: ZnO crystalline Structures:

(a) Cubic rocksalt (B1), (b) cubic zinc blende (B3), and (c) hexagonal wurtzite (B4). Shaded gray and black spheres denote Zn and O atoms, respectively [14].

Zinc oxide in the form of wurtzite structure is very stable under normal atmospheric temperature and pressure. Hence, the wurtzite structure is the most common stable crystal structure. For zinc blende structure, it can be stabilized by growing it on cubic substrates. In addition to the two forms of zinc oxide structures mentioned above, zinc oxide also crystallizes in the rocksalt structure under high hydrostatic pressure. It is also possible for the wurtzite structure to transform to the rocksalt structure when a pressure of about 9 GPa is applied [14].

Figure 1.1 above shows that wurtzite and zinc blende structures have no symmetry inversion, i.e the reflection of a given crystal with respect to any point does not transform it to itself. This property makes the two structures exhibit piezoelectricity, since piezoelectricity is due to linear electromechanical interaction existing between the mechanical and electrical state of a crystal material that shows no inversion symmetry.

Zinc oxide in the wurtzite crystal structure has a hexagonal unit cell and it is characterized by the two lattice parameters *a* and *c* as shown in Fig 1.2, with a ratio of *c/a* =1.633. The wurtzite structure is composed of two interpenetrating hexagonal close packed sub-lattices. In each of the sub-lattices, each of the atoms is displaced in relation to one another along the three fold *c*-axis with a magnitude of *u* = 3/8 = 0.375.

This *u* parameter, defines the bond length, which is also represented by b/c where *b* is the nearest-neighbor distance, and the value is 0.375 in ideal crystal structure. In Fig 1.2, α and β bond angles with a value of 109.47^{o} in ideal crystal. However, real zinc oxide crystal structure has a deviation from the standard arrangement, by altering the ratio *c/a* or the value of *u*. There exists a relationship between the ratio *c/a* and *u.* For example, when the value of *u* parameter increases, the value of *c/a* decreases in a way that the tetrahedron distance remains fairly constant, perhaps only the tetrahedron angle is distorted as a result of long range polar interactions [14].

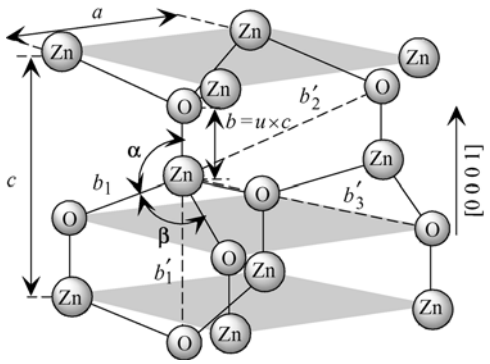

Figure1.2: Schematic diagram of a wurtzite ZnO crystal structure. *a* and *c* stand for lattice constants in the basal plane and basal direction, respectively [14].

1.2 Defect Structures of Zinc Oxide.

In order to fully understand how the performance of a semiconductor device can be enhanced, it is important to examine the crystal structure in general and the significant role played by defects and impurities.

Crystalline materials generally show a periodic crystal structure. The locations of the atoms occur at regular fixed distances, which are dependent on the parameters of the unit cell. However, there is often deviation from perfect orderliness of the crystals. The orderliness is interrupted by crystallographic defects [15]. In zinc oxide, these structural defects play a major role on the optical, electrical and structural properties. Hence it is pertinent that we examine each kind of defect in order to understand how to use these defects to control the properties of zinc oxide

- Vacancy defects: In an ideal crystals lattice, the atoms are arranged in an exact periodic order, but often in a real crystal, an atom may be vacant from a particular lattice site. This defect is called a vacancy. The movement of nearby atoms to the vacant position will make the vacancy move in the opposite direction to the site which used to be occupied by the moving atoms. In some cases, the atoms in the vicinity of the vacancy move away from the vacancy because they experience an attractive force from the atoms in the neighborhood [15].
- Interstitial defects: This kind of defect occurs when an atom occupies a location that is not usually occupied in the crystals structure. When there is a close pair of an interstitial and a vacancy we have a defect called a Frenkel defect, which usually results when an ion moves into an interstitial site and

creates a vacancy. Interstitial and vacancy defects affect the crystal structure by breaking the ideal geometric orderliness, and distorting the ideal chemical bonding between the atoms. Consequently, this leads to drastic changes in the electrical and optical properties of the material [15].

- Substitutional defects: This kind of defect occurs when an impurity atom occupies a regular site in the crystal structure. In substitutional defects, no vacancies and interstitials are created. The substituted atom is considered as an impurity because it is not supposed to be in the newly occupied site. There is often a mismatch between the radii of the removed atom and the substituting atom, which consequently makes the equilibrium position drift away from the lattice site. This kind of defect is sometimes called off -center ions because the equilibrium position of the substituted ions has drifted away from their regular lattice site [16].

- **Complexes:** This can be formed between different kinds of point defects. For instance, if an impurity encounters a vacancy, the two may bind together if the impurity is too large for the lattice. Interstitials can form 'split interstitial' or 'dumbbell' structures where two atoms effectively share an atomic site, resulting in neither atom actually occupying the site [15-17]. The various types of defects are illustrated in Fig. 1.3.

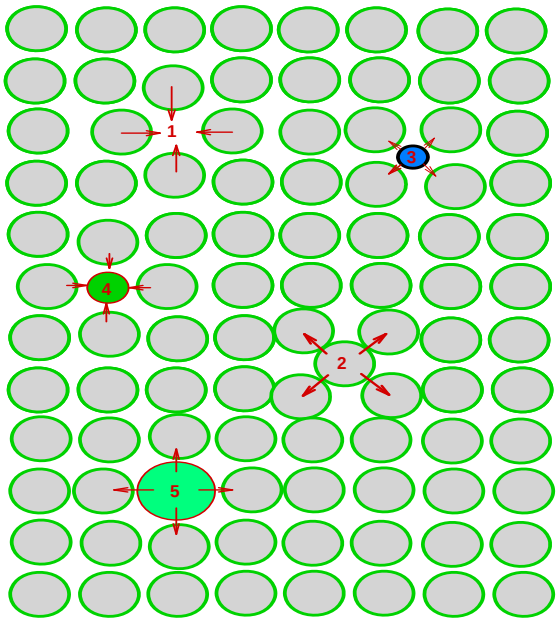

Figure 1.3: Various kinds of crystal defects. (1) vacancies, (2) self-interstitial, (3) interstitial impurity, (4,5) substitutional impurities. [16].

1.3 Literature review:

In search for the adaptability of zinc oxide for optoelectronic and transparent conducting oxide applications, extensive experimental research work has been conducted to unravel some unclear questions pertaining to the conductivity of zinc oxide. Zinc oxide is predicted to be an intrinsic semiconductor. However, it almost exclusively occurred naturally as *n* type. The cause of this natural semiconductivity is still unclear.

In order to address the problem, enormous studies have been carried out to determine the effects of various parameters such as doping, annealing ambient, annealing temperature, and growth conditions that could alter the basic properties such as optical, electrical,

structural and chemical properties. Of critical importance is the deposition technique employed in the growth process of zinc oxide thin films.

Radio frequency (RF) magnetron sputtering has been established as the most widely used technique for the fabrication of zinc oxide thin films. This stems from four reasons (i) Ease of operation, (ii) Too many parameters to control the properties of the films, (iii) It leads to high quality films, and (iv) It can be adapted for large scale production. The Influence of the deposition parameters on the properties of RF sputtering has been extensively investigated. In what follows, I review the work conducted on post-deposition annealing of RF-sputtered ZnO films.

Chang *et al.*[18] investigated the effect of post deposition annealing in different ambients (air and hydrogen) on Al–doped zinc oxide thin films. The substrates used were SiO_2/Si and glass, and the substrate temperature was 200 ^oC. The minimum resistivity obtained in the experiment was 8.76×10^{-4} Ω .cm, for the films annealed in hydrogen at 500 ^oC for 1 hour. The group reported that the resistivity of the films annealed in air increased drastically.

Keunbin *et al.*[19] observed that the electrical resistivity of zinc oxide films deposited on glass decreased as the temperature and annealing time increased when the ambient was a reducing one (N_2+5%H). The minimum resistivity of 4.9×10^{-4} Ω.cm was achieved when the annealing temperature was 200 ^oC for 15 hours. The group explained that the decrease in resistivity was due to the passivation of grain boundaries and also the passivation of zinc ions by hydrogen atoms leading to an increase in carrier concentration and mobility. In addition, they noted that the optical transmittance was not improved by

annealing. The optical band gap widened or narrowed when annealing in reducing atmosphere or oxidizing atmosphere, respectively. The widening of the band gap was attributed to blue shift decrease in wavelength.

Chang *et al.* [20] studied the effect of annealing and thickness on the properties of Ti: ZnO thin films prepared on substrates heated to 300 ^{o}C. The electrical, optical, and structural properties were investigated. It was found from XRD analysis that all the films exhibited the (002) peak. The researchers suggested that the films possessed hexagonal wurtzite structure with *c*-axis orientation perpendicular to the substrate. It was also noted that as the thickness of the films increased from 30 to 950 nm, the crystallite size and the surface roughness changed from 11.9 to 36.8 nm and 0.57 to 1.78 nm, respectively. Furthermore, it was established that the resistivity of the film reduced from 3.94×10^{-2} Ω.cm to 1.06×10^{-3} Ω.cm. The annealing was carried out at a temperature range of 300-500 ^{o}C in hydrogen and argon ambient for transparent conducive oxide applications. The results indicated that with hydrogen annealing, the resistivity decreased with annealing time, while the decrease in resistivity due to argon annealing was less pronounced.

Charpentier *et al.*[21] examined the effect of post-deposition annealing atmosphere (vacuum, N_2+5%H_2, pure N_2) and temperature (within the range of 400-500 ^{o}C) on the optical, electrical, and microstructural properties of ZnO: Al thin films. The following observations were made:

(i) When pure nitrogen was used as the annealing gas, the film showed an increase of grain size through XRD measurement. When the annealing temperature increased it was observed that there was a drop in charge carrier concentration and Hall

mobility, which culminated into an increase in resistivity. The limitation in the grain barrier transport was due to the integration of acceptor center at the boundaries and in the bulk.

(ii) For annealing under vacuum, the films showed a small increase in band gap. Also, there was an increase in grain size with an increase in charge carrier concentration which led to reduction of barrier height at the grain boundaries. Hence, an improvement on electrical conductivity for the films annealed in vacuum was observed.

(iii) For films annealed in an N_2/H_2 atmosphere, a strong increase of the charge concentration was associated to an increase of the optical band gap, as well as a decrease of the resistivity. However, the increase of the Hall mobility was strongly limited by bulk limited transport, resulting from ionized impurities and phonon scattering.

The effect of H_2/Ar and vacuum annealing on zinc oxide was also reported by Jwayeon *et al* [22]. The following observations were noted:

(i) They found that as the annealing temperature in hydrogen/argon and vacuum increased, there was a decrease of mobility and resistivity of zinc oxide films

(ii) The values of resistivity obtained were 768 Ω.cm and 2186 Ω.cm when the films were annealed at 300 ^{o}C in vacuum and Ar/H_2 ambient respectively.

(iii) At 600 ^{o}C annealing temperature, the values of resistivity were roughly

0.035 Ω.cm and 0.04 Ω.cm in H_2/Ar and vacuum ambient, respectively.

(iv) It was established that the role of hydrogen as a dominant donor was more significant than the role of oxygen vacancy or interstitial zinc donor.

(v) They also reported that the average optical transmittance was 82 % for all the films annealed in both ambient,

(vi) They also established that the preferred orientation was (002) peak.

Changgang *et al.*[23] examined the influence of hydrogen annealing on the electrical, optical and structural properties on indium-doped zinc oxide thin films. The following observations were reported:

(i) The crystallinity of the films may be degraded when they were hydrogen annealed.

(ii) When the annealing temperature was above 350 ^{o}C, the surfaces of the film was damaged.

(iii) The surface roughness decreased after annealing the films.

(iv) The transparency obtained in the visible and infrared was within 80-90 %.

(v) There was a decrease in the resistivity from $1.25\times10^{-3}\Omega$.cm to

$6.7\times10^{-4}\Omega$.cm, when the films were annealed in hydrogen.

(vi) By changing the hydrogen annealing duration and temperature, the work function could be varied between 4.6-4.98 eV.

Hyun *et al*.[24] examined the role of oxygen vacancy on annealed ZnO thin films deposited in hydrogen and argon ambients. They investigated the role played by hydrogen on the electrical and physical properties of ZnO film annealed at 300 ^{o}C in relation to oxygen vacancies. The following observations were reported

(i) In both annealing ambients (Ar and H_2), the carrier concentration was increased.

(ii) In the Ar gas ambient, the mobility was decreased drastically, while in the H_2 ambient the decrease was quite small.

(iii) The physical structure of ZnO was unchanged, irrespective of the annealing ambient. The crystalline orientation was the (002) wurtzite structure.

1.4 Scope of Work:

There have been quite a large number of studies on zinc oxide and its use in various semiconductor and electronics applications. Most of the work has been on ways to enhance the basic properties such as electrical, optical and structural properties. The aim of this work is to study the effect of substrate temperature and hydrogen annealing on the properties of zinc oxide thin films prepared by RF magnetron sputtering. The films will be deposited on unheated substrates as well as substrates heated to 400^{o}C. Annealing will be carried out under hydrogen atmosphere in the temperature range 300-600^{o}C. For most research on zinc oxide, the annealing temperature has been fixed at a certain temperature. My studies will investigate the effect of these parameters on the electrical, optical, structural, and chemical properties of films.

CHAPTER TWO

EXPERIMENTAL TECHNIQUES AND DETAILS

This Chapter highlights the various experimental techniques employed in the course of this work. The film deposition was carried out by RF magnetron sputtering and as such it's pertinent to discuss the underlining principles in RF magnetron sputtering. The various experimental procedures used in the characterization of the films will also be discussed.

2.1 SPUTTERING

Sputtering is a thin film deposition technique that is utilized by several industries in the manufacturing of optical, semiconductor, and optical disk devices. On the atomic scale, sputtering can be defined as the process in which atoms are ejected and then deposited on a substrate by bombarding the source material with energetic particles. These energetic particles are created by ionization of the sputtering gas which usually is an inert gas. The resulting ionized charged particles is referred to as the plasma. Depending on the source of power supply fed to the target material, sputtering can be classified into the following:

- Direct current (DC) sputtering
- Alternating current (AC) sputtering
- Radio frequency (RF) sputtering.

The latter two technique are used in the deposition of insulating materials. In this work, RF magnetron sputtering was used for the deposition of the films.

2.2 RF MAGNETRON SPUTTERING

Magnetron sputtering uses strong magnetic and electric fields to confine the plasma generated in close proximity of the target material, which thus increases the intensity of bombardment by the ions. The plasma is created by the application of RF power, hence the technique is called RF magnetron sputtering. Figure 2.1 shows a schematic diagram of RF magnetron sputtering.

The general working principle of RF magnetron sputtering can be broken down into four essential stages:

- Creation of vacuum with the aid of a turbo molecular pump.
- Generation of ionized particles by application radio frequency power which subsequently bombard the target material.
- Acceleration of the ions towards the target.
- Deposition on the substrate.

Argon gas was introduced through a mass flow controller into the deposition chamber where the substrates were placed, the application of RF power creates the plasma. Since these ions are charged particle, their motions were controlled by the magnetic field. The interaction of the ions with the target leads to sputtering and hence deposition on the substrate [25].

2.3 THIN FILMS DEPOSITION AND PROCESSING

2.3.1 Thin Film deposition

Thin film deposition was carried out by radio frequency magnetron sputtering with the aid of an Oerlikon Univex 350 sputtering system. The target was zinc oxide of 3-inch diameter with a purity of 99.9 % (Vin karola). The substrates were cleaned with acetone in an ultrasonic bath, in order to remove contaminants from the surface of the substrate before deposition. The sputtering power was set at 150 W, and the source- to-substrate distance was 10 cm. First, the initial pressure of the deposition chamber was reduced to 1.0×10^{-5} mbar with the aid of a turbo molecular pump. This was followed by introduction of the sputtering gas (argon with 99.9% purity) at a flow rate of 20 sccm (standard cubic centimeter per minute). At this point the pressure inside the chamber was decreased to 1.5×10^{-2} mbar.

The films were deposited simultaneously on two different substrates: fused silica and molybdenum. The substrates were rotated at a speed of 6 rpm to ensure uniformity in film thickness. Film preparation was done in two different categories. The first set of substrates was unheated, while the second set was heated to 400 ^{o}C. Duration for the deposition in both cases was 2 hours. The films were labelled according to the designation below:

F1-As: As deposited films without substrates heating

F1-300: Films deposited on unheated substrates and annealed at 300 ^{o}C

F1-400: Films deposited on unheated substrates and annealed at 400 ^{o}C

F1-500: Films deposited on unheated substrates and annealed at 500 ^{o}C

F1-600: Films deposited on unheated substrates and annealed at 600 ^{o}C

F2-As: As deposited films with substrates heating

F2-300: Films deposited on heated substrates and annealed at 300 ^{o}C

F2-400: Films deposited on heated substrates and annealed at 400 ^{o}C

F2-500: Films deposited on heated substrates and annealed at 500 ^{o}C

F2-600: Films deposited on heated substrates and annealed at 600 ^{o}C

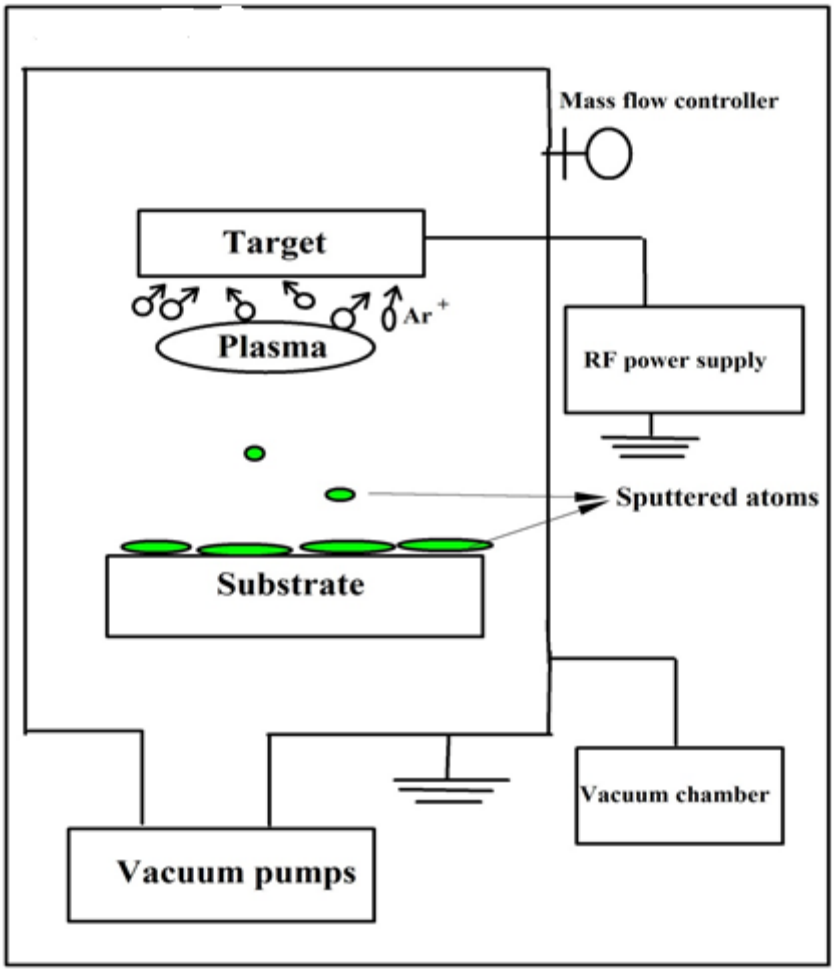

Figure 2.1: Schematic diagram of RF magnetron sputtering system.

2.3.2 Annealing of the films

The deposited films were annealed in a horizontal tube furnace that uses a digital temperature regulator (see Fig 2.2). We used the regulator to control the annealing temperature from 300-600 ^{o}C and also to control the annealing duration according to cycle shown in Fig 2.3. The films were annealed in hydrogen. The annealing temperature was raised at the rate of 7 min / ^{o}C. The flow rate was set to 100 sccm with the aid of a flow meter. Before the annealing was carried out, the furnace was first evacuated to a base pressure of 2×10^{-4} mbar using a combination of roughing and turbo-molecular pumps in order to remove any form of gaseous impurities that may affect the films properties. After each of the annealed films was heated to the desired temperature and duration, the samples were allowed to cool down to room temperature before they were removed.

It is important to note that no films were found on the substrates after annealing at 500 or 600 ^{o}C. This is an indication that the films were completely removed (etched) by annealing under hydrogen ambient. Previous studies have reported that ZnO films were completely etched in hydrogen ambient when annealed at temperatures equal to or higher than 500 ^{o}C [19,21,32]. In my case, this is even more pronounced because of the extended annealing time. Therefore, in the remainder of my discussion, only as deposited films and those annealed at 300 or 400 ^{o}C will be presented.

Figure 2.2: Furnace used for the annealing.

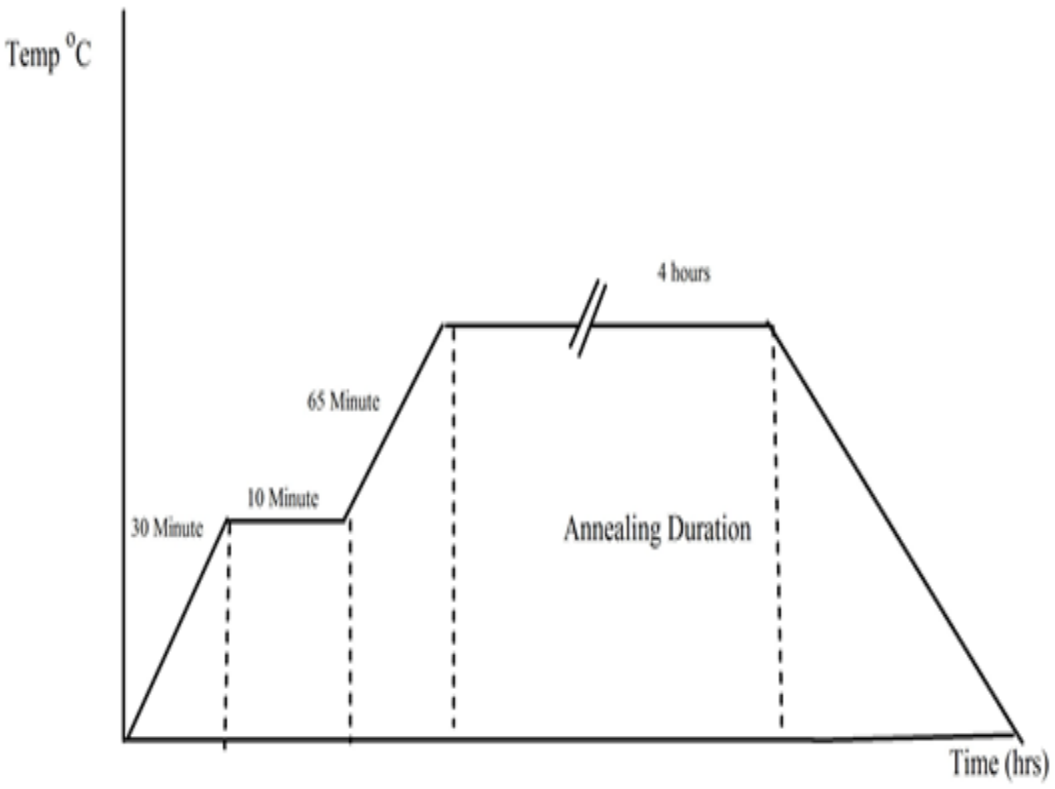

Figure 2.3: Annealing process chart.

2.4 CHARACTERIZATION TECHNIQUES

The properties of the films were investigated using various characterization techniques mentioned below.

2.4.1 **Structural Analysis**

X-ray diffraction (XRD) is a powerful technique that was used in the investigation of the structure of our films. Parameters that one can obtain from XRD analysis include the following: (i) Crystallographic structure. (ii) Crystallite size (iii) Preferred orientation of the crystal structure, and (iv) Lattice parameters.

Working principle**:** The main idea in XRD is Bragg's law. When an electromagnetic wave that has a wavelength comparable to atomic dimensions is incident on a crystalline sample, the reflected rays will undergo constructive interference if the Bragg's law is satisfied. The points of constructive interference correspond to certain crystallographic orientation [26].

As shown in Fig 2.4, when an incident X ray hits the planes of the crystal, the rays are diffracted. The path length difference between diffracted rays over any successive planes must differ by an integer multiple (m) of wavelengths for constructive interference to occur. Mathematically, it can be shown that the condition for Bragg diffraction is given by

$$m\lambda = 2\tau sin\theta \qquad (2.1)$$

where τ the interspacing distance between successive planes and the angle of incidence is θ.

The structure of our films was investigated by XRD using a Rigaku Ultima IV diffractometer, employing Cu K_α (1.54 Å) radiation. The 2θ scan range was performed from 20^o to 80^o with 2θ step of 0.02^o and with step acquisition time of 1.0 s

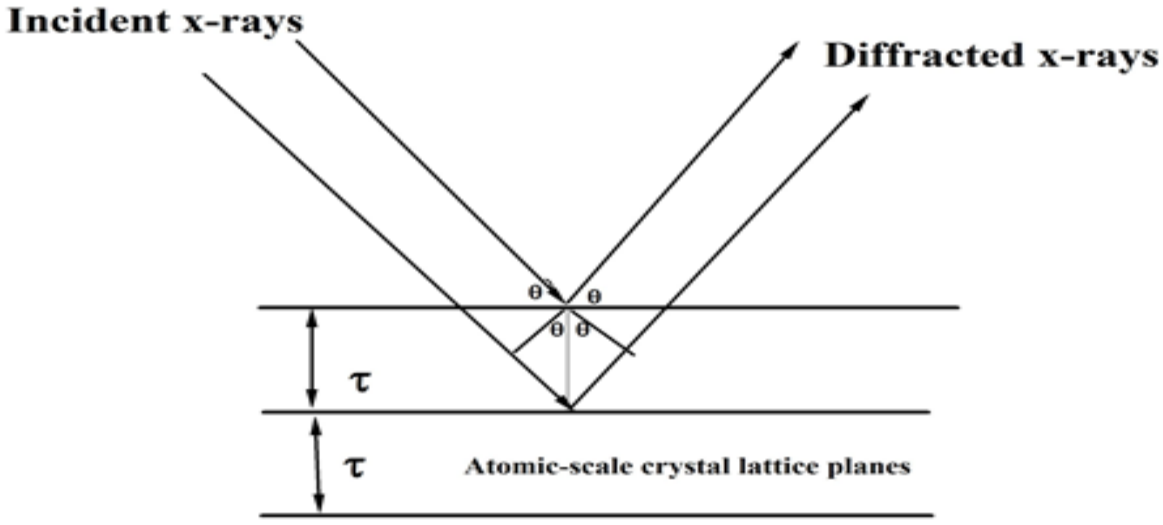

Figure 2.4: Schematic Diagram of Bragg's law of diffraction

2.4.2 Surface morphological analysis

Atomic force microscopy (AFM) was used for measuring and imaging the surface of our samples. It is generally used to investigate surface morphology with a resolution capability of the order of a nanometer.

Working Principle:

For the analysis of our films, we operated the AFM (Veeco Innova diSPM) in the non-contact mode which is suitable for semiconductor analysis. The scan area is $5\mu m \times 5\ \mu m$. The essential components of the AFM are shown in Fig 2.5. The main components consist of the following:

(i) A cantilever with a sharp nano silicon size tip (10nm)

(ii) A laser beam

(iii) A photo detector

(iv) Feedback mechanism system

(v) Computer

At the start of operation of the AFM, the tip of the cantilever approaches the film surface. An attractive force exists between the tip and the film surface at a certain distance. This attractive force causes the deflection of the tip by the sample which automatically deflects the cantilever.

The cantilever oscillates at it resonance frequency (300 kHz). As it moves over the film surface, the attractive force causes fluctuation in its resonant frequency. The feedback mechanism restores the resonance frequency of the cantilever by making appropriate adjustment of the distance between the tip and the film surface, in such a way that it value is held constant [28]. A laser light is incident on the cantilever as shown in Fig 2.5. As the cantilever oscillates because of varying attractive force between the tip and the film surface, the intensity of reflected laser light varies, the variation is captured by photo a detector which is then converted to a topological map with the aid of a computer.

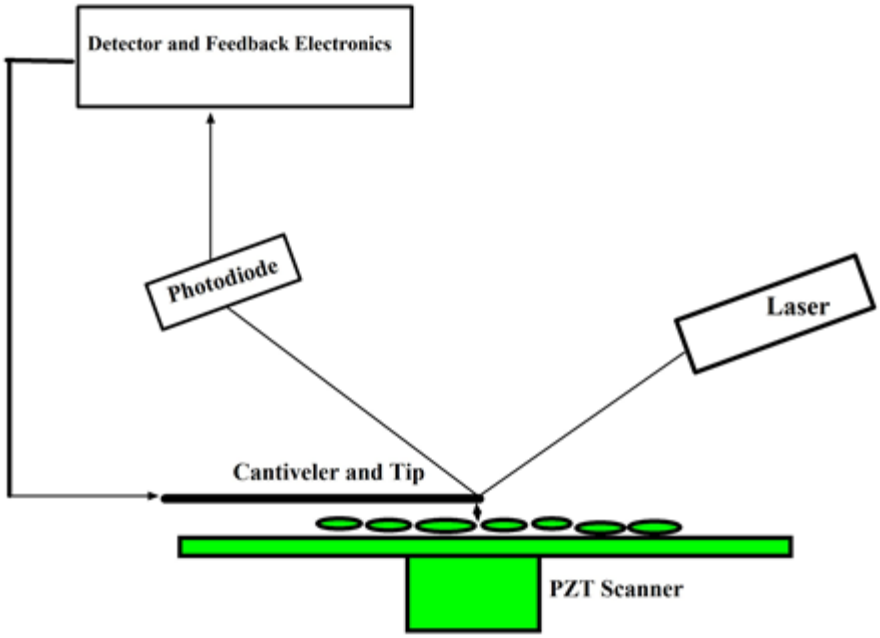

Figure: 2.5 Schematic diagram of atomic force microscopy [29].

2.4.3 Optical measurement

Optical analysis of films involves the determination of the optical band gap, absorption coefficient, and thickness. In order to determine these parameters transmittance and reflectance were measured using a Jasco V-570 double beam spectrophotometer. The range of wavelength chosen was between 200-1200 nm.

Double beam spectrophotometer: A spectrophotometer is a device that is used to measure the intensity of light as a function of its wavelength. A double beam spectrometer compares the light intensity between two light path, one path containing the reference

beam and the other the test sample. Light sources, diffraction gratings, filters, photo detectors and signal processors are the various parts of a spectrophotometer.

Figure 2.6 shows the schematic diagram of a double spectrophotometer. The light source provides light with wavelength in visible, ultra-violent, and near infrared ranges. The filters and diffraction grating separate the light into its component wavelengths so that a very small range of wavelength can be directed onto the sample. The sample compartment permits the entry of no stray light while at the same time without blocking any light from the source. The photo detector converts the amount of light which it had received into a current which is then sent to a signal processor. The signal processor converts current into reflectance or transmittance which is then sent to the display.

In transmission measurement the spectrophotometer quantitatively compares the amount of light that passes through the reference beam and the sample. For reflectance, the spectrophotometer compares the amount of light reflected from the reference and the sample.

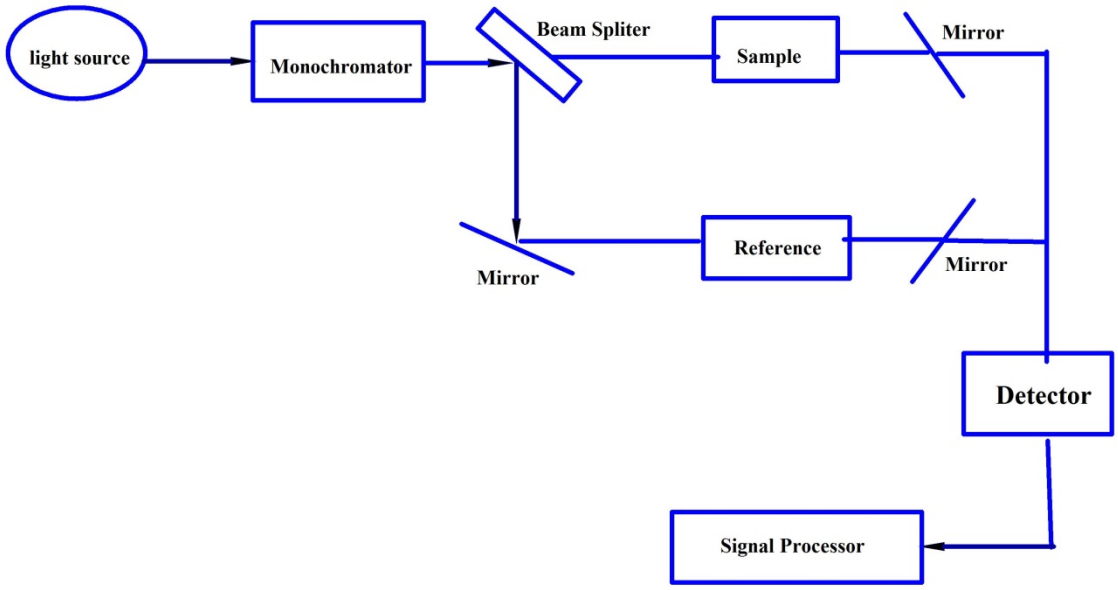

Figure 2.6: Schematic diagram of a double beam spectrophotometer

2.4.4 Resistivity measurement

We used the Van der Pauw technique for determining the resistivity of our films. The following parameters were obtained using van der Pauw technique and Hall effect measuring system.

- Resistivity
- Mobility
- Carrier concentrations

These parameters are essential characteristics in any potential transparent conducting oxide applications.

We made the contacts with the aid of a conducting fluid, a silver paste, and thin conducting chromium wires were used for connecting the four edges. The assembly was soldered and mounted on a small modular printed circuit board which goes into our Hall

Effect measuring system from where the necessary measurements were obtained. The model of the instrument used was Ecopia Hall effect measurement (HMS-3000).

The resistivity of the films is given by

$$\rho = dR_s \tag{2.2}$$

where R_s is the sheet resistance and d represents the thickness. R_s can be obtained from the equation below.

$$e^{-\pi \mathrm{R}A/\mathrm{Rs}} + e^{-\pi \mathrm{R}B/\mathrm{Rs}} = 1 \tag{2.3}$$

where R_A is the resistance obtained by passing the current from point 1 to 2 and measuring the voltage from terminal 3 and 4. Similarly, R_B is obtained by passing current from point 2 to 3 and measuring the voltage from point 4 and 1 (see Fig. 2.7) [30]. Mathematically, the resistances are given below :

$R_A = V_{43}/I_{12}$ and $R_B = V_{14}/I_{23}$

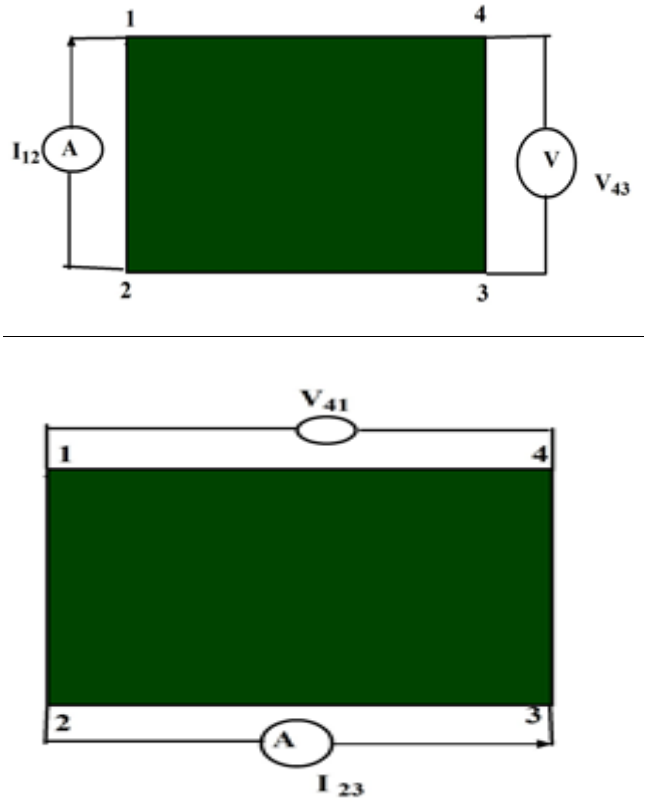

Figure 2.7: Arrangement for Van der Pauw technique.

2.4.5 X-ray photoelectrons spectroscopy

X-ray photoelectron spectroscopy (XPS) is a chemical analytic technique that is used to analyze the surface chemistry of a material. The experiment was performed in a Thermos

Scientific Escalab 250Xi spectrometer equipped with a monochromatic Al K_α (1686.6 eV) x-ray source. The instrumental energy resolution was 0.5 eV with an x-ray spot size of 650-μm diameter. During the XPS analysis, the samples were maintained at ambient temperature at a pressure of 5×10^{-8} Pa.

XPS technique provides detailed information on the chemical composition of the surface, usually down to depth of 1 to 10 nm. On this account, XPS is often regarded as a surface sensitive analytic technique.

Besides hydrogen and helium, XPS detects all other elements of the periodic table. This is related to small absorption cross section of hydrogen and helium.

Basic principle of XPS

Figure 2.8 illustrates the fundamental concept in XPS. When an x-ray photons is incident on a material, photoelectrons are ejected from the inner core shell (k). Electrons are bounded to different orbitals through their respective binding energy with respect to the nucleus. For photoelectrons to be ejected, the incident x-ray energy has to exceed the sum of the binding energy and work function of the spectrometer. The excess energy is given to the liberated electrons as kinetic energy.

From the law of conservation of energy, we can deduce the governing equation as

$$hv = B.E + W_f - K_e \quad (2.4)$$

By rearranging equation (2.4), we have

$$B.E = hv - W_f - K_e \quad (2.5)$$

where hv is the energy of the x-ray used (Al K_α source). K_e is the kinetic energy of the ejected electrons, which is obtained from the measured velocities of the electrons. W_f is a fixed constant referred to as the work function of the spectrometer.

The above equation is valid if the ejected photoelectrons do not suffer losses as a result of scattering with other electrons on their way to the surface. A typical XPS spectrum is a plot of the count of photoelectrons detected as a function binding energy. Every element has a unique set of peaks at certain values of binding energy. It is important to highlight that the observed peaks in XPS spectrum result from photoelectrons emitted near the surface. These photoelectrons did not suffer collisions prior to their escape from the surface of the material.

Photoelectrons liberated from depth beyond 3-10 nm are more likely to suffer from inelastic collisions with phonons and other electrons in the material. As a result, a significant portion of their energy will be lost before reaching the surface. These electrons contribute to the background in the XPS spectrum.

A schematics diagram for the principle involved in XPS is shown Fig 2.8 below [31].

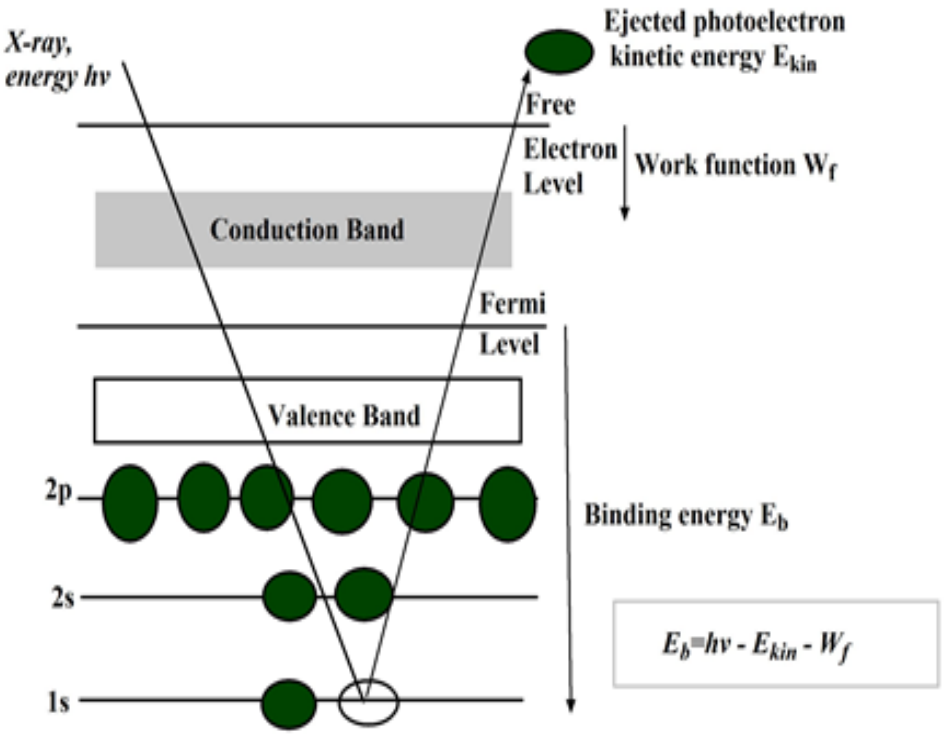

Figure 2.8: Schematic diagram of interaction of photons with core level electrons in XPS technique [31].

CHAPTER THREE

STRUCTURAL PROPERTIES

3.1 Thickness and deposition rate

The thickness of the films was determined from the maxima and minima of transmittance spectra. A typical transmittance spectrum (see Fig 3.1) manifests maxima and minima that result from interference between the two light beams reflected from the two interfaces of the film (with air and substrate). The thickness (d) of the film is given by

$$d = \frac{\lambda_1 \lambda_2}{4n(\lambda_1 - \lambda_2)} \tag{3.1}$$

where λ_1 is the spectral position of a maximum (or minimum), λ_2 is the spectral position of an adjacent minimum (or maximum), and n is the refractive index of the film. The refractive index is determined from the value of the transmittance at the minimum (T_{min}), using the relation:

$$n = 4.22-(2.94\ T_{min}) \tag{3.2}$$

The values of the thickness determined from the above equation are given in the Table (3.1) below

Several observations can be made regarding the thickness of the films:

(i) The thickness of the as-deposited films was reproducible up to 3% or 4% for films deposited on unheated or heated substrates, respectively.

(ii) The deposition rate was 5.7 or 4.2 nm/min for the films deposited on unheated or heated substrates, respectively. This may indicate re-evaporation of the material sputtered onto heated substrates.

(iii) There was a slight decrease in thickness upon annealing at 300 ^{o}C. This indicates that the films became compact, as supported by the slight increase in refractive index.

(iv) On the other hand, there was a slight increase in thickness when the films were annealed at 400 ^{o}C. This may indicate the formation of larger grains via the aggregation of small grains or grain boundaries.

Table 3.1: Values of the thickness of the films.

Sample	F1-As	F1-300	F1-400	F2-As	F2-300	F2-400
d (nm)	681	655	704	502	495	528
n	1.83	1.84	1.82	1.89	1.91	1.88

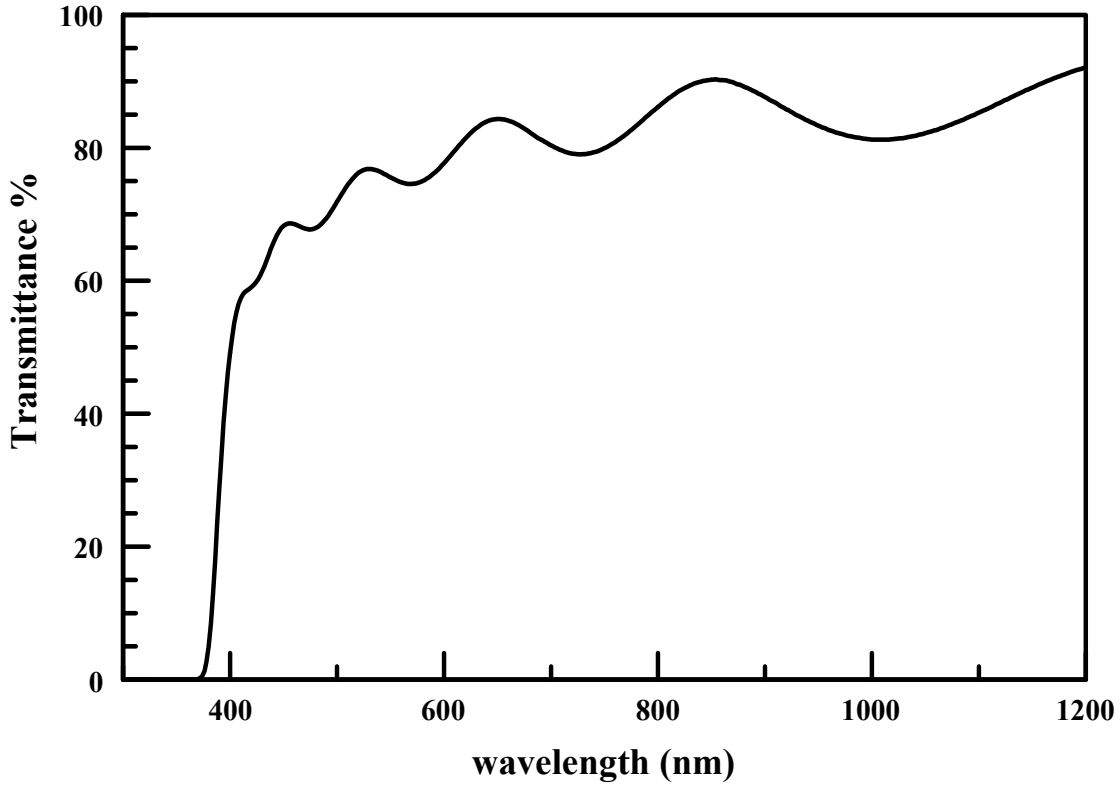

Figure 3.1: A typical transmittance spectrum.

3.2 X- RAY DIFFRACTION (XRD) ANALYSIS

Figures 3.2 and 3.3 show the XRD patterns of all the films deposited on unheated and heated substrates, respectively. Identification of the peaks was based on the international center for diffraction data (ICDD) file number 01-076 -0704. The as-deposited films on unheated substrate exhibited a polycrystalline structure having the (002) and (101) orientations of the hexagonal structure of ZnO. It is well known that the (002) direction, i.e. the *c* axis, is the preferable orientation commonly observed in ZnO prepared by

various deposition techniques. In the case of hexagonal ZnO, the surface energy density of the (002) direction is the lowest, indicating that (002) texture of the films may easily form [33, 34]. The as-deposited films on heated substrates exhibited better crystallinity with an oriented growth along the (100) direction. It is clear that substrate heating has altered the energetics of crystalline growth in favor of this direction. This may be attributed mainly to the higher deposition rate in our experiments. A similar observation was reported in the literature for ZnO films prepared by atomic laser deposition [35] and electrochemical deposition [6].

The crystalline quality of the films was evaluated by the crystallite Size (L), which was estimated using Debye-Scherrer formula:

$$L = \frac{0.9\lambda_{\alpha}}{\Gamma \cos\theta} \qquad 3.3$$

where λ_{α} is the wavelength of the Cu K_{α} x- ray radiation (1.54 Å), Γ is the full width at half maximum of the XRD peak, and θ is the corresponding diffraction angle [33,36]. The most intense peak in each spectrum was used to calculate the crystallite size, and the values are shown in Table 3.2. It is evident that annealing enhanced crystalline growth.

Several observations can be made regarding the crystallite size, as follows:

(i) The crystallite sizes ranged from 7 to 17 nm, which reflects the nano-crystalline nature of the films.

(ii) The films deposited on heated and unheated substrates exhibit polycrystalline growth as seen from the several peaks on the XRD patterns. This is highly

related to the rapid deposition rate in my experiments, which does not allow enough time for adatoms mobility during sputtering [37].

(iii) The crystallite size increased for the as deposited films on heated substrates. Improved crystallinity is due to the increase in adatoms mobility of sputtered species on the surface of the substrate, which is enhanced by deposition on a heated substrate [37].

(iv) Heating of the substrates resulted in switching of the most preferred growth direction. (002) was the most preferred direction for unheated substrate while (001) peaks was the preferred growth direction for the heated substrates.

(v) For a given substrate temperature, the crystallite size increased upon annealing. Thus, annealing in hydrogen results in promotion of crystal growth due to heating [38].

(vi) The enhancement of crystallinity with annealing was much pronounced in the films deposited on unheated substrates. This is because the (002) direction is the most preferable direction for crystalline growth in ZnO [18].

(vii) The intensity of the (002) and (100) peaks for the unheated and heated substrates, respectively, do not change noticeably after the annealing temperature was increased from 300 ^{o}C to 400 ^{o}C.

(viii) As- deposited films on unheated substrates suffer from internal compressive stress. due to the shifting of the 002 peaks from the bulk 2θ value towards lower angles. However, upon annealing, the residual stress in the films were relaxed as evidenced, by shifting the XRD peak patterns towards higher angles. This stress is typical for films deposited by sputtering [39].

Table 3.2: Values of the crystallite sizes of the films and diffracting angles

Films	*FI-AS*	*F1-300*	*F1-400*	*F2-AS*	*F2-300*	*F2-400*
$2\theta^{o}$	33.84	34.63	34.41	31.42	31.34	31.57
L (nm)	7.5	16.1	16.3	10.2	13.1	13.2

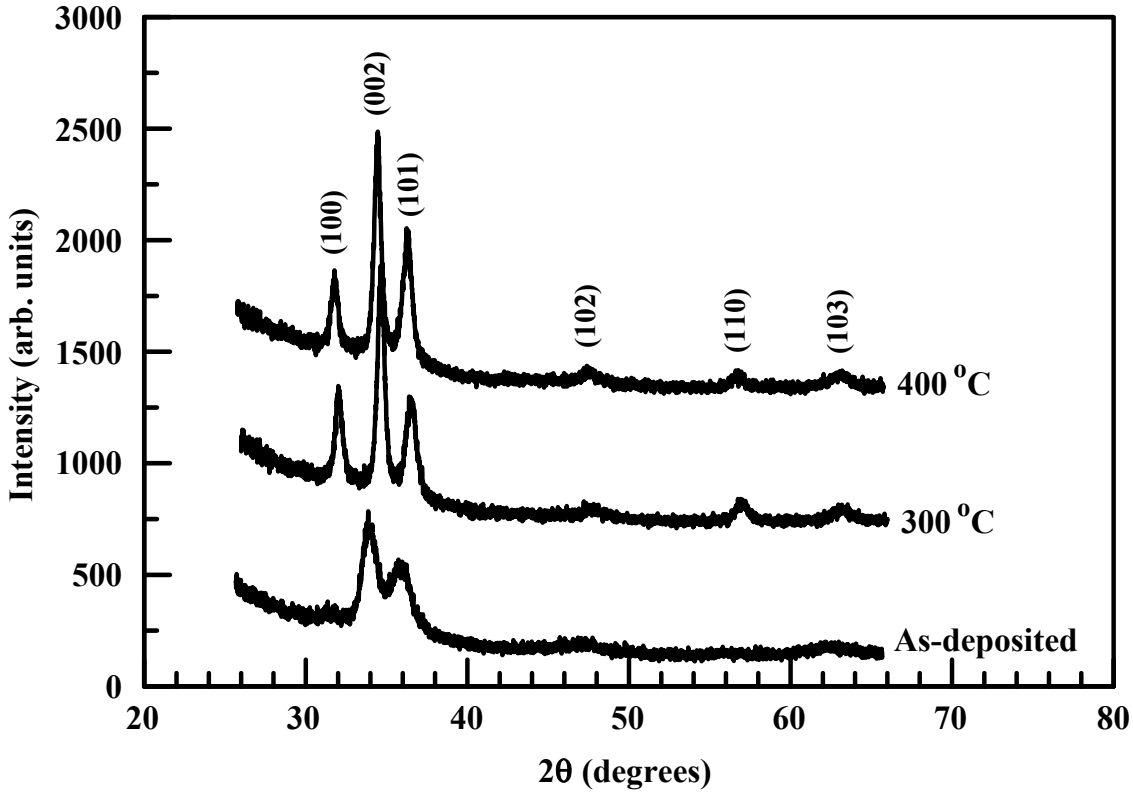

Figure 3.2: XRD patterns for films deposited on unheated substrates, and further annealed at 300 ^{o}C or 400 ^{o}C.

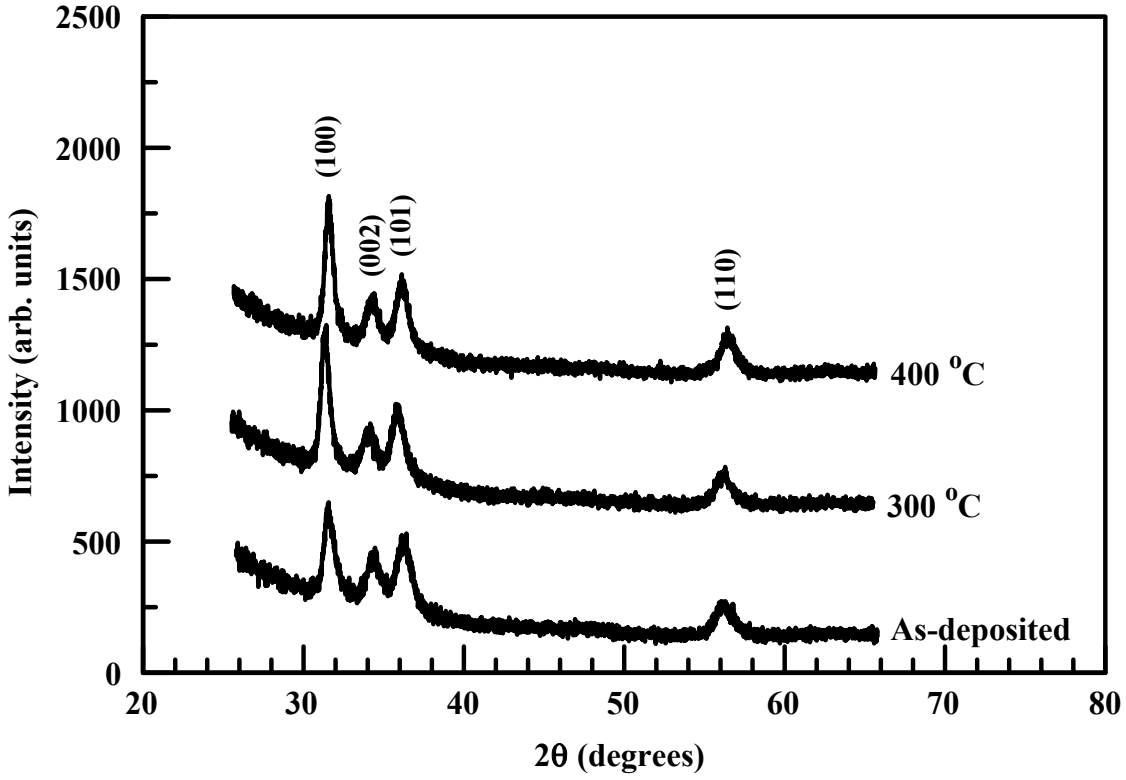

Figure 3.3: XRD patterns for films deposited on heated substrates, and further annealed at 300 ^{o}C or 400 ^{o}C.

3.3 MORPHOLOGICAL ANALYSIS

Atomic force microscopy (AFM) was used to characterize the morphology and film growth mode, and also to estimate the surface root-mean square roughness *(R_{rms})* and lateral grain size (σ). Two-and three-dimensional AFM images of the films are shown in Figures 3.4 and 3.5, for the films deposited on unheated and heated substrates, respectively. The results on surface roughness and lateral grain size are given in Table 3.3. On the nano-scale, the films deposited the both substrates (heated and unheated) exhibited non uniformity and rough surfaces. The growth pattern for the as-deposited and annealed films on the unheated substrate was columnar. However, the patterns for heated substrates were granular. Our values of the surface roughness are comparable to those of films deposited by RF magnetron sputtering [40].

For the as- deposited films, the surface roughness decreased as the substrate temperature was increased. This is due to the enhanced mobility of atoms diffusing to lower energy sites on the surface, which subsequently reduced surface roughness [41]. The increase in surface roughness may be attributed to enhanced growth of lateral grain size upon annealing [42]. This assumption is consistent with our films, except for the films deposited on unheated substances and annealed at 300 ^{o}C. In summary, substrate temperature seems to play the dominant role in magnitude of surface roughness.

Table 3.3*:* Morphological analysis of the films

Sample	F1-As	F1-300	F1-400	F2- As	F2-300s	F2-400
R_{rms}	24.5	27.1	26.6	12.8	14.8	16.0
σ (nm)	61	58	62	56	59	62

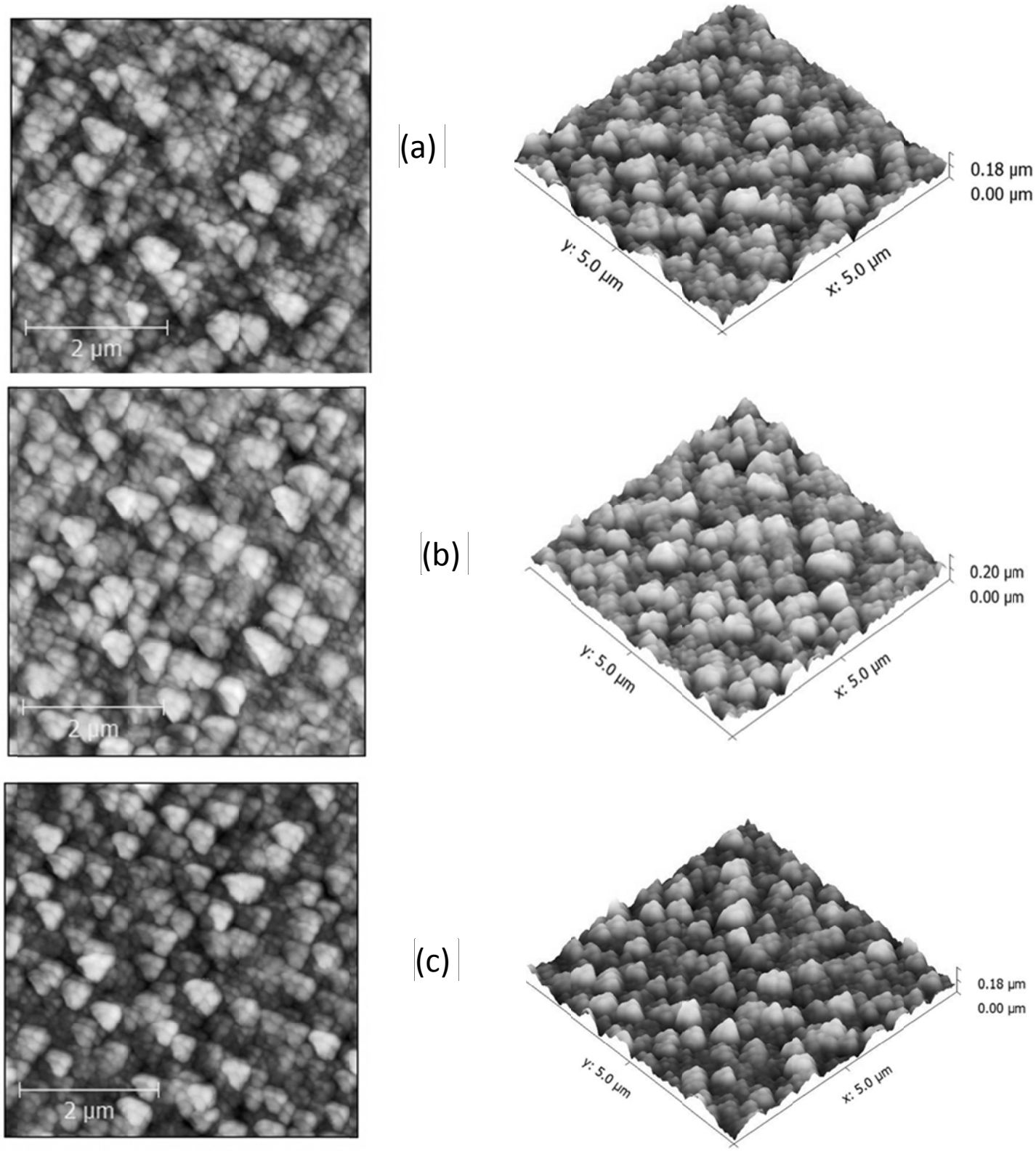

Figure 3.4: Two dimensional (left) and three dimensional (right) AFM images of the films deposited on unheated substrates: (a) As-deposited, (b) annealed at 300 oC, (c) annealed at 400 oC.

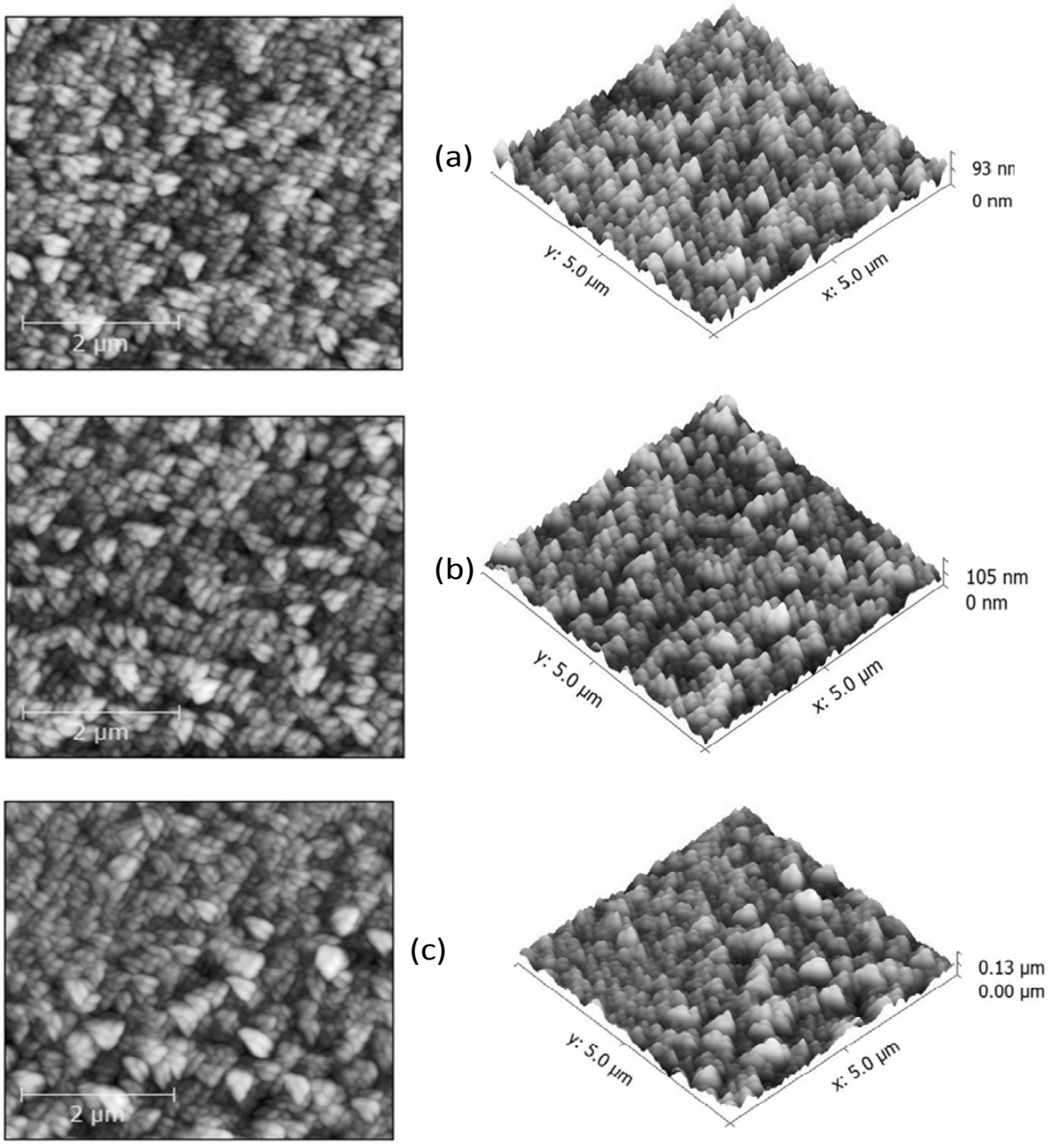

Figure 3.5: Two dimensional (left) and three dimensional (right) AFM images of the films deposited on heated substrates:(a) As-deposited (b)annealed at 300 ^{o}C(c) annealed at 400 ^{o}C.

CHAPTER FOUR

CHEMICAL ANALYSIS

Chemical analysis of the sample was carried out with the aid of x-ray photoelectron spectroscopy. Figure 4.1 shows a typical XPS survey spectrum of a ZnO thin film. The survey scan provides a quick identification of the constituent elements present in the sample. High resolution spectra were obtained for zinc, oxygen and carbon. While the zinc and oxygen are from the deposited samples, the carbon is from atmospheric contamination and is usually referred to as adventitious carbon. Other visible peaks that appeared in Fig 4.1 are related to Auger electrons peaks (Zn LMM, O KLL) [43]. A typical spectrum for C 1s is shown in Fig 4.2. The binding energy of the main C 1s peak at 284.6 eV was used as the reference for other spectra. The smaller carbon peak at 288.5 eV is due C-O and C=O bindings [40]. For XPS analysis, the films were deposited on tantalum substrate, in order to reduce the charge shift.

Detailed information on the chemical state of the sample's constituent elements was obtained from the high resolution spectra. Figure 4.3 shows a representative scan of the zinc 2p spectrum for films deposited on unheated substrates. All the zinc 2p core level spectra exhibited two sublevels due to spin orbit splitting [40]. The corresponding values of the Zn 2p binding energies are shown in Tables 4.1 and 4.2. The results obtained agreed with the reported values for the Zn $2p_{3/2}$ and $2p_{1/2}$ levels, which are (1021.5-1022.4) eV and (1044-1045) eV, respectively [41]. As seen from the figures, the Zn 2p spectra were symmetric, which indicates that Zn exists only in the oxidized state [40].

Each oxygen O1s spectrum as shown in Fig 4.4 and 4.5 was de-convoluted into three components and fitted using Gaussian with appropriate subtraction of shiley type background [24]. The three components are designated as low binding energy (LBE), Intermediate binding energy (IBE), and high binding energy (HBE). This designation is based on the reported range of binding energies of each of the components. The reported range of values for each of the components is given below:

(i) low binding energy (LBE) ranges from (529.7- 530.5) eV [42]

(ii) Intermediate binding energy (IBE) ranges from (530.8-531.6) eV [42]

(iii) High binding energy (HBE) ranges from (532-534) eV [42]

The low binding energy is attributed to O^{2-} ions on the wurtzite structure of the hexagonal Zn^{2+} ions arrays [23]. This component relates to the oxygen in the zinc oxide lattice. The intensity of this component relates to the amount of oxygen in a fully oxidize state. The intermediate binding energy is related to the oxygen in the oxygen-deficient regions in the ZnO matrix. The variation in the relative intensity of this component with respect to the total O 1s intensity is related to the concentration of oxygen vacancies in ZnO [24] . The high binding energy is due to adsorbed or chemisorbed oxygen from (OH) and CO_3^{2-} . This component is mainly from atmospheric contamination [1,44] .

Tables 4.1 and 4.2 show the calculated relative weight of each of the oxygen components in the O 1s spectrum for the films deposited on unheated and heated substrates, respectively. The weight of a component was obtained by dividing its area by the total O 1s area.

4.1 Chemical Analysis of films deposited on unheated substrates.

The as-deposited films were highly stoichiometric when compared to annealed films. However, upon annealing at 300 ^{o}C, more oxygen vacancies were created. This can be seen from the reduction in the low binding energy (LBE) component from 57 to 34 %. When the annealing temperature was increased to 400 ^{o}C, the oxygen vacancy increased further, thereby reducing the LBE component of O 1s to 13 percent.

On the other hand, the intermediate binding energy component which is related to the concentration of oxygen vacancies, showed a consistent increase intensity. This is expected since the annealing was carried out under a reducing atmosphere.

In addition, the HBE component for the as-deposited films had large intensity, which is indicative of their porosity. Examination of its AFM images confirms the presence of large pores in the as-deposited films. Densification of the films upon annealing at 300 ^{o}C led to reduction in the porosity of the films, and hence a reduction in the HBE component. Annealing the films at 400 ^{o}C, resulted into almost complete removal of the HBE component.

4.2 Chemical Analysis of the films deposited on heated substrate:

The as-deposited films on heated substrate showed a reduction in the low binding energy component, and an increase in the oxygen vacancy component when compared with the as-deposited films grown on unheated substrates. This can be attributed to out-diffusion of oxygen in the lattice at elevated substrate temperatures [45].

The LBE component was reduced when the films were annealed at 300 ^{o}C, as expected for annealing under a reducing ambient. However, upon annealing at 400 ^{o}C, there was a relative increase in the LBE component from 40 %, for as-deposited films to 54 % for the films annealed at 400 ^{o}C. This increase does not imply that more oxygen was attached to the zinc atoms in the lattice during hydrogen annealing. Rather, it resulted from the major decrease in the HBE component from 29 to 0.02 %.

There was a progressive but slight increment in the *IBE* component. This is an indication that as the annealing temperature increased, more oxygen vacancy were created. This is in good agreement with our results for the films deposited on unheated substrates.

After annealing in hydrogen at 400 ^{o}C, the HBE component of O 1s was reduced to an insignificant level. Meaning that chemisorbed oxygen that act as traps for carriers at the boundaries was removed completely.

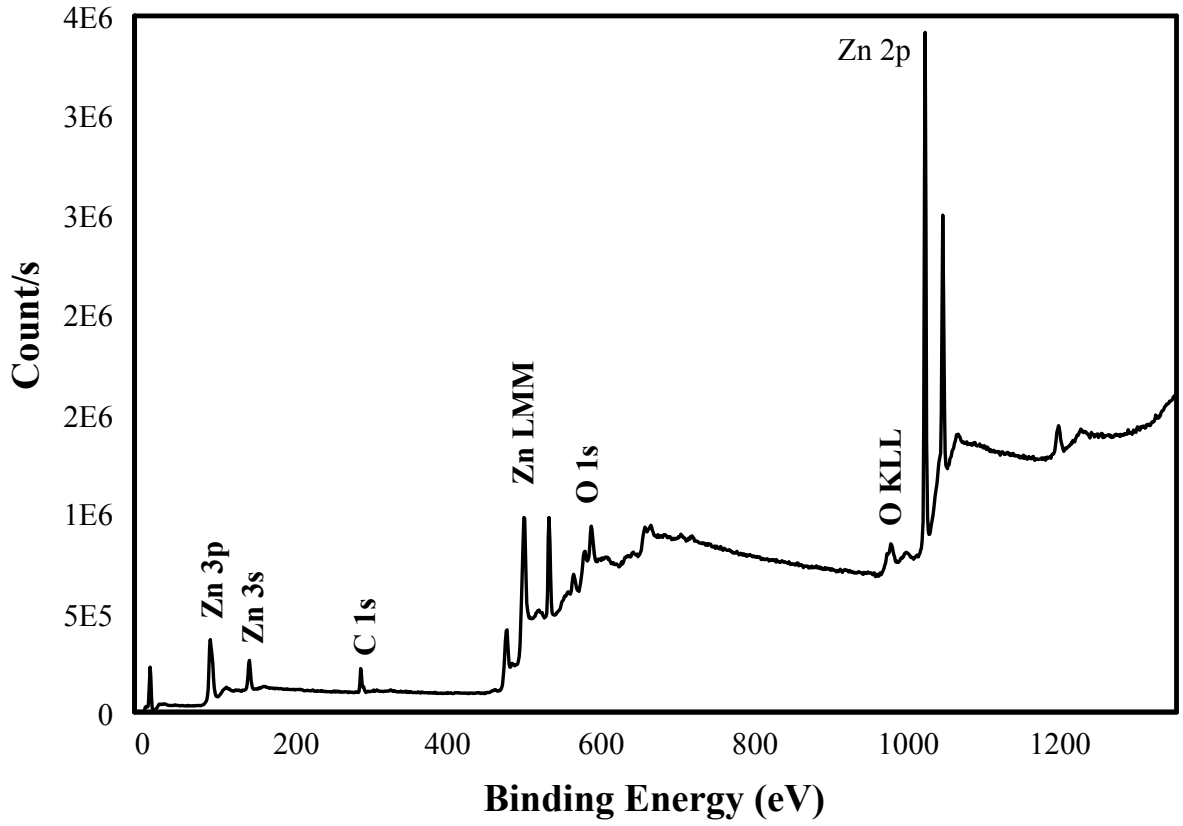

Figure 4.1 : A typical Survey spectrum for ZnO thin film sample

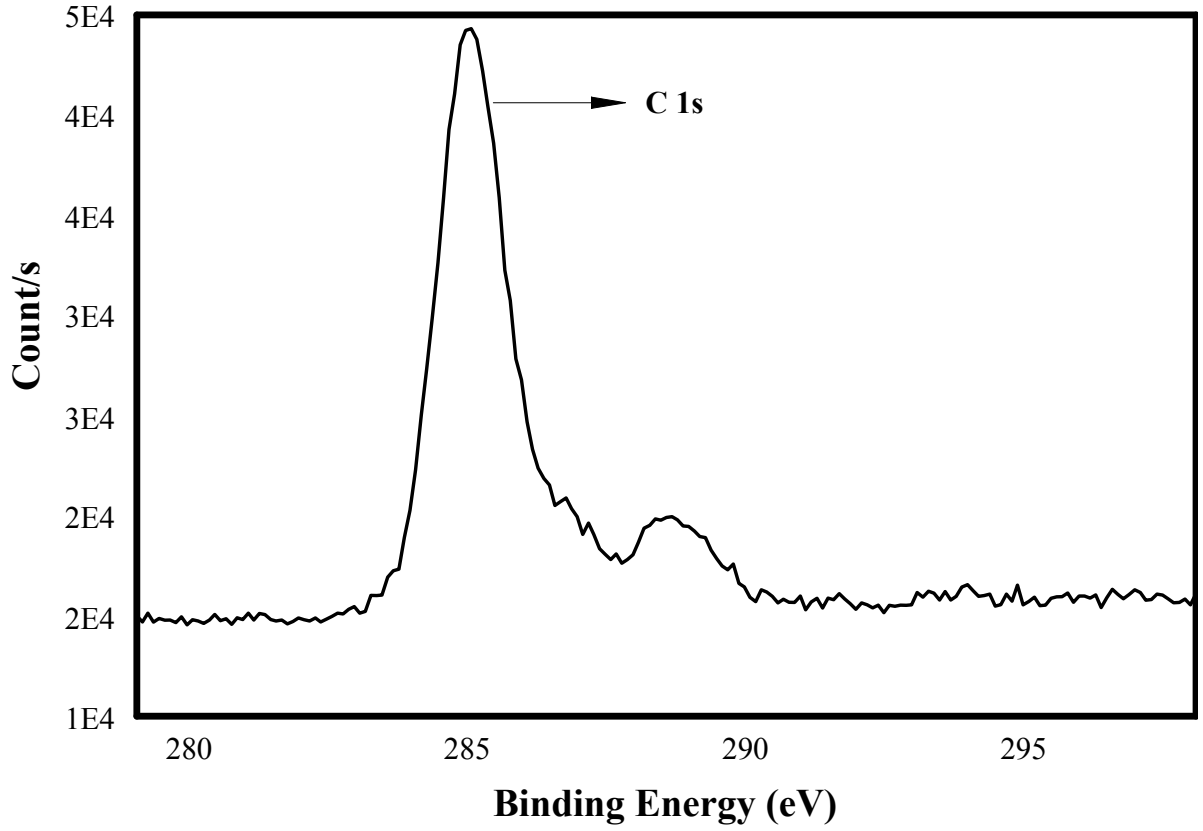

Figure 4.2: Adventitious C 1s spectrum

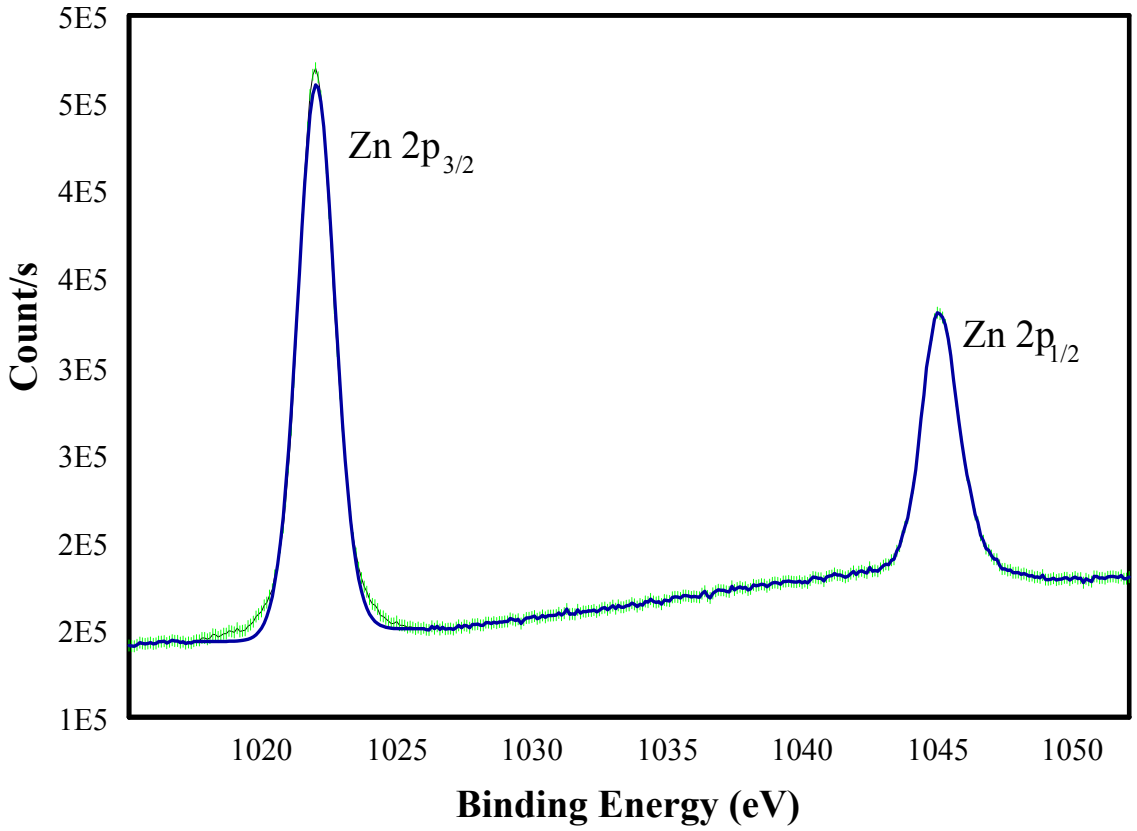

Figure 4.3: A typical XPS spectrum for zinc 2p for films deposited on unheated substrates.

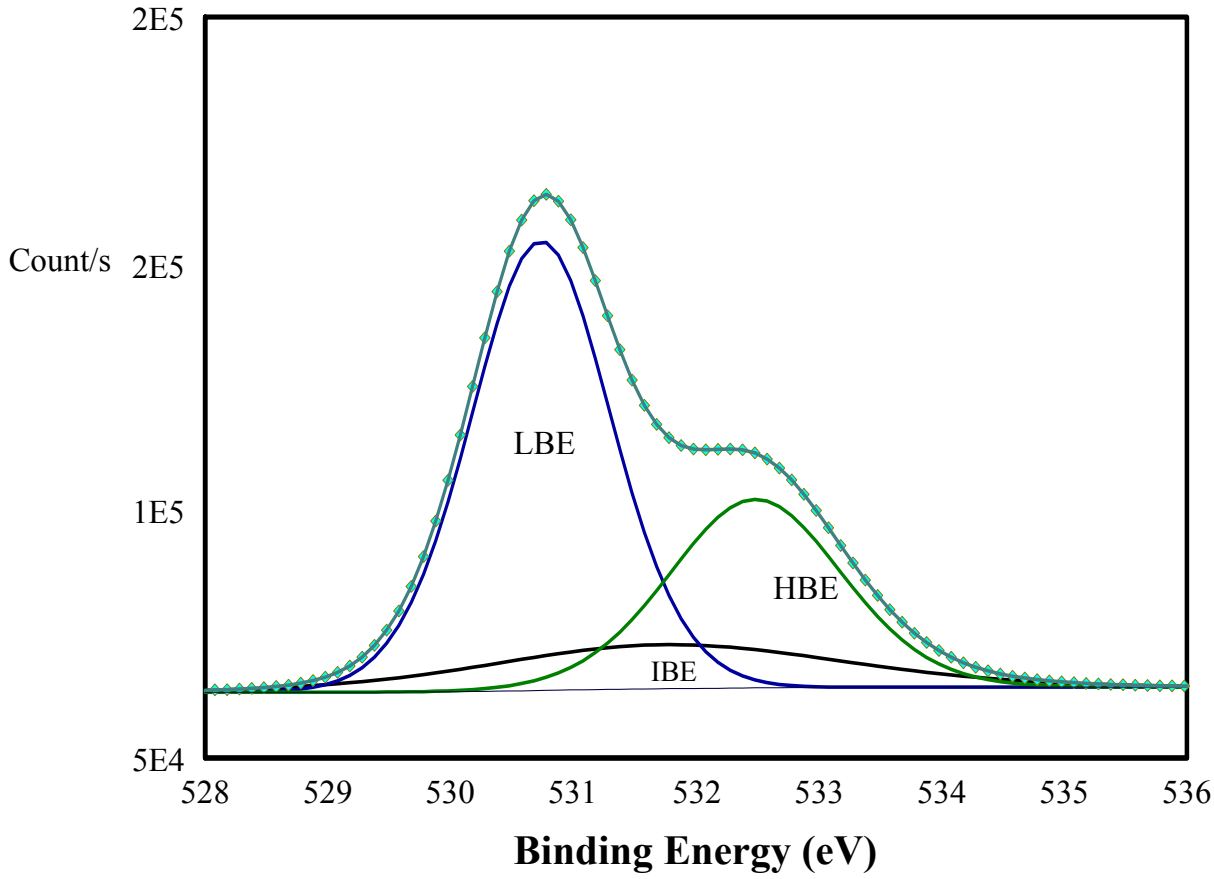

Figure 4.4: XPS spectrum of O 1s showing its various components for the as-deposited film grown on unheated substrate.

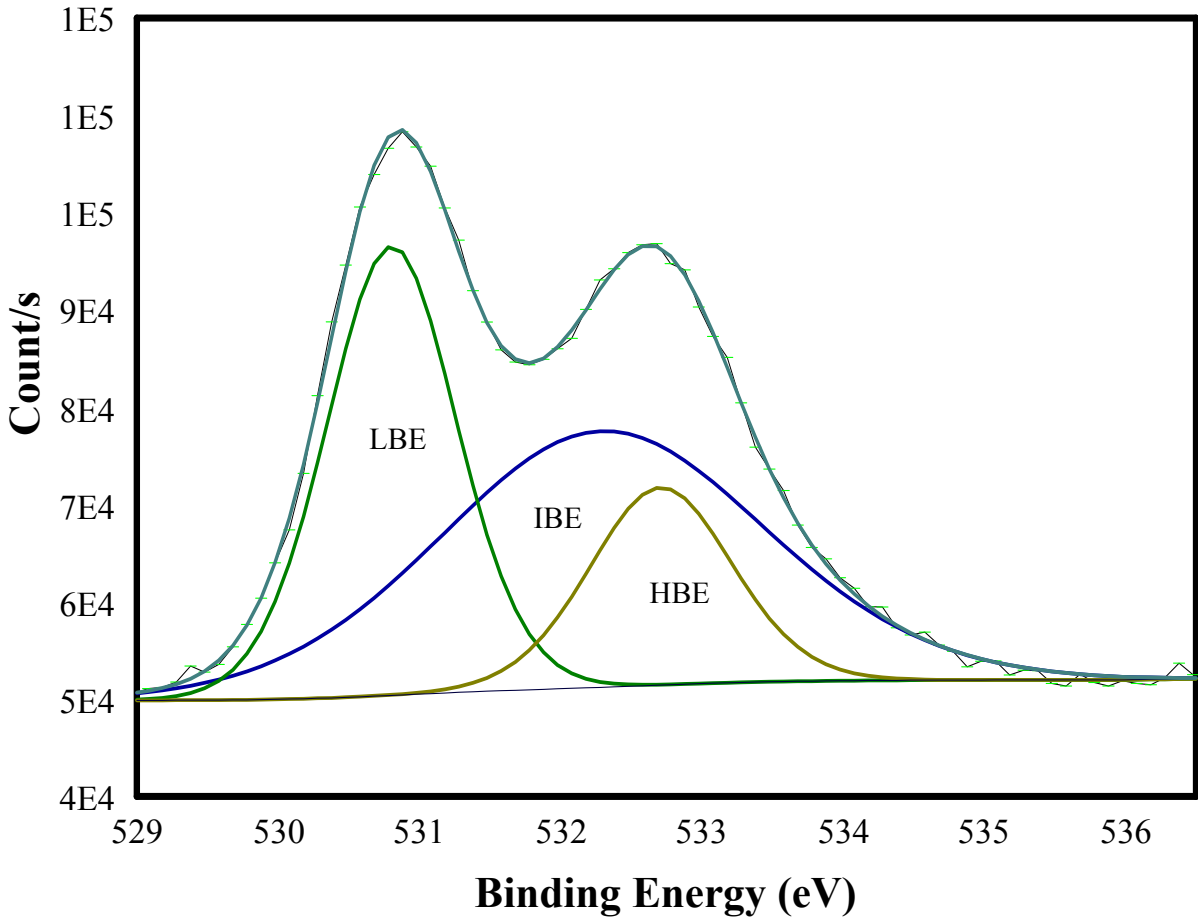

Figure 4.5: XPS spectrum of O 1s showing its various components for the film deposited on unheated substrate and annealed at 300 ^{o}C.

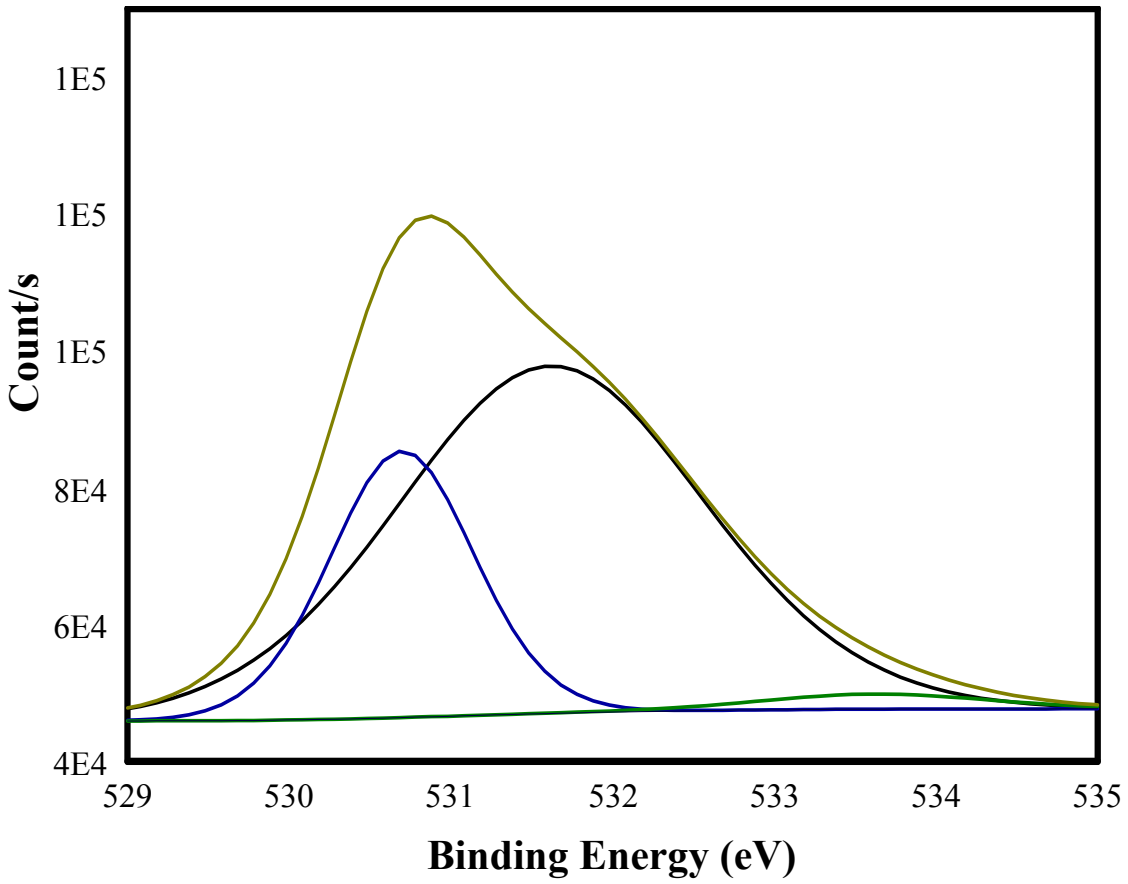

Figure 4.6: XPS O 1s spectrum showing various components for the film deposited on unheated substrate and annealed at 400 oC.

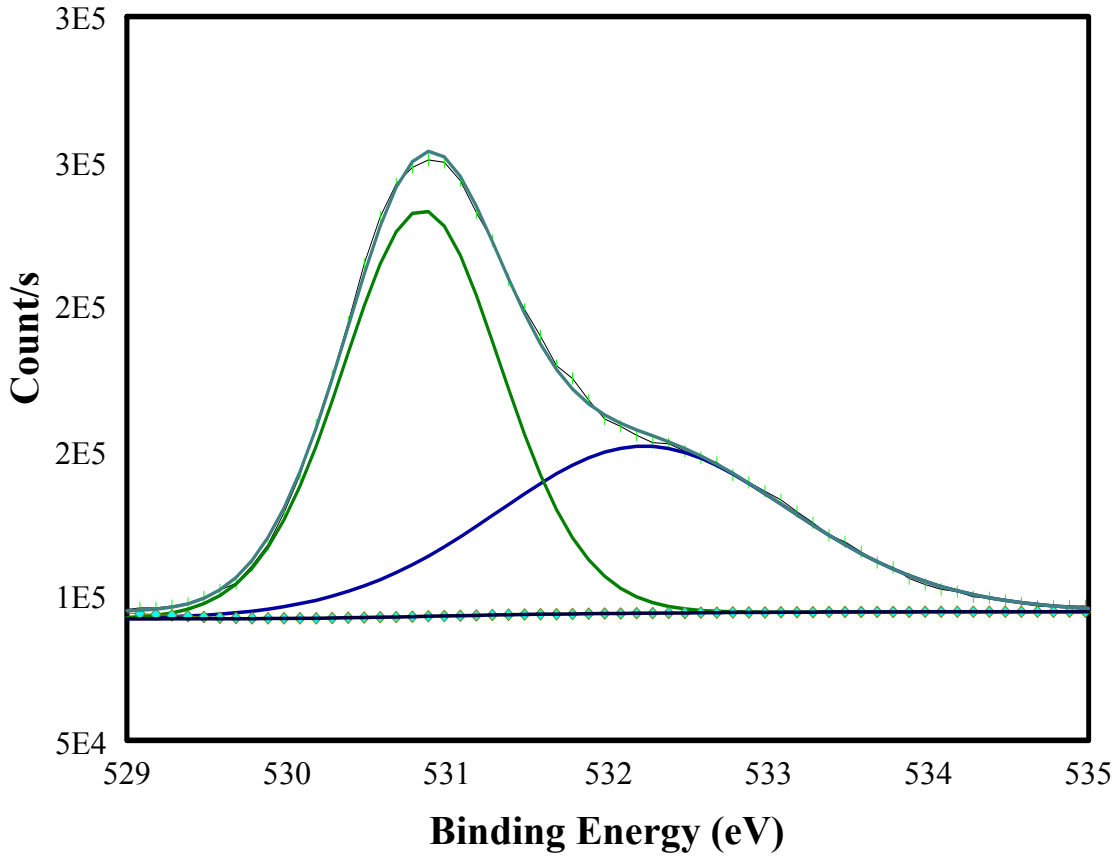

Figure 4.7: XPS spectrum of O 1s showing its various components for the as-deposited film grown on heated substrate.

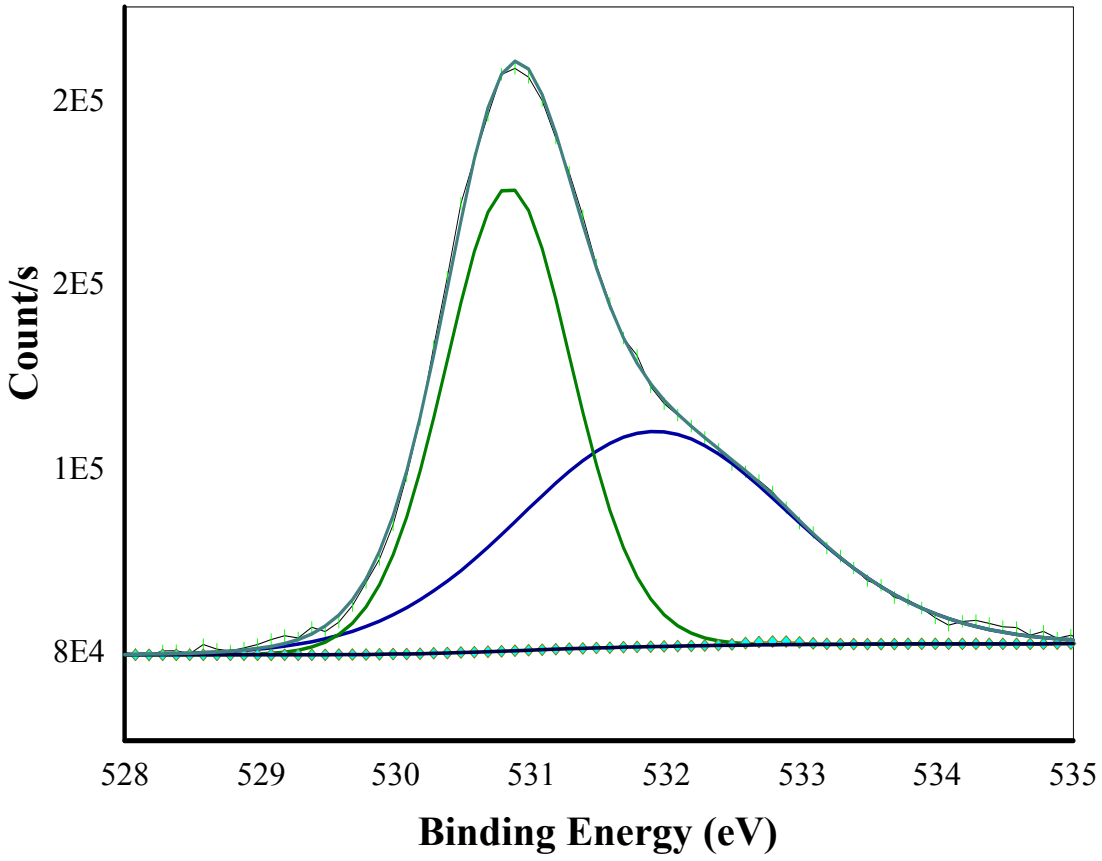

Figure 4.8: XPS spectrum of O 1s showing its various components for film deposited on heated substrate and annealed at 300 ^{o}C.

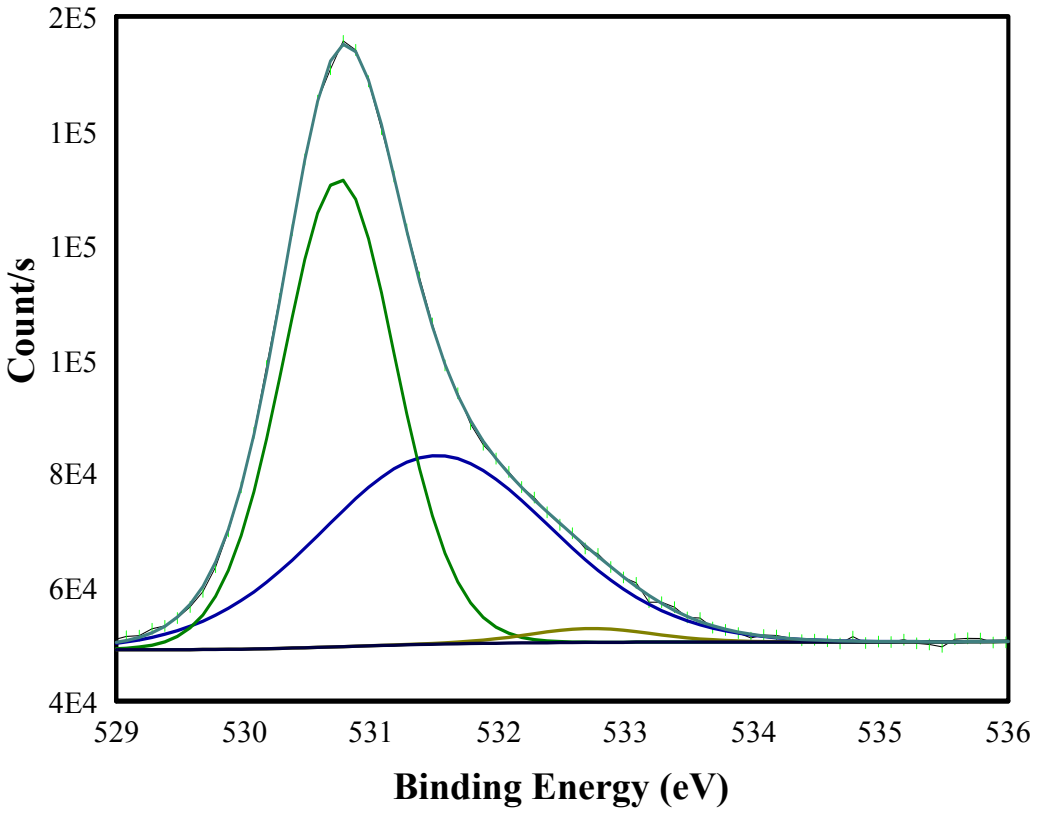

Figure 4.9: XPS spectrum of O 1s showing its various components for film deposited on heated substrate and annealed at 400 ^{o}C.

Table 4.1: XPS results for the films deposited on unheated substrates

As- deposited films						
Elements	Component	Binding Energy (eV)	Γ(eV)	Area	Relative Percentage of O1s components	Δ
O	LBE	529.80	1.36	133776.50	0.57	491.50
	IME	530.80	3.37	30668.80	0.13	490.50
	HBE	531.60	1.67	69916.40	0.30	489.70
Zn	Zn $2p_{3/2}$	1021.30	1.97	1243575.00		
	Zn $2p_{1/2}$	1044.30	1.97	644134.90		
	χ	23.0				
Films annealed at 300 ^{o}C						
O						
	LBE	530.00	1.09	54334.40	0.34	491.40
	IBE	531.50	2.72	77494.30	0.49	489.90
	HBE	531.90	1.19	26174.30	0.17	489.50
Zn	Zn $2p_{3/2}$	1021.40	1.77	384843.30		
	Zn $2p_{1/2}$	1044.40	1.77	199337.40		
	χ	23.0				
Films annealed at 400 ^{o}C						
O	LBE	530.20	1.05	44451.50	0.26	491.30
	IBE	531.10	2.24	123444.20	0.72	490.40
	HBE	533.10	1.63	3908.72	0.02	488.40
Zn	Zn $2P_{3/2}$	1021.50	1.7	569093.30		
	Zn $2P_{1/2}$	1044.50	1.7	294773.50		
	χ	23.0				

Γ: Full width at half maximum, LBE: Low binding energy component, IME: Intermediate binding energy component, HBE: High binding energy component, χ is the separation between the energies of the Zn 2p spin orbit split and Δ is the difference in binding energy values between zinc $2p_{3/2}$ and the LBE component of O 1s.

Table 4.2: XPS results for films the deposited on heated substrates

As- deposited films						
Elements	Component	Binding Energy (eV)	Γ(eV)	Area	Relative percentage of O1s components	Δ
O	LBE	529.80	1.06	126118.70	0.40	492.00
	IME	530.40	1.86	126176.30	0.40	491.90
	HBE	531.80	1.73	64408.20	0.20	490.50
Zn	Zn $2p_{3/2}$	1022.30	1.91	1499462.00		
	Zn $2p_{1/2}$	1045.30	1.91	776677.00		
	χ	23.0				
Films annealed at 300 ^{o}C						
O						
	LBE	529.80	1.00	88462.60	0.28	491.50
	IBE	530.20	1.54	137208.10	0.43	491.10
	HBE	531.70	1.84	89997.20	0.29	489.60
Zn	Zn $2p_{3/2}$	1021.30	1.82	1026321.00		
	Zn $2p_{1/2}$	1044.30	1.82	531603.80		
	χ	23.0				
Films annealed at 400 ^{o}C						
O	LBE	530.20	1.05	93524.80	0.54	491.30
	IBE	530.90	2.15	77053.90	0.44	490.50
	HBE	532.10	1.14	2963.70	0.02	488.30
Zn	Zn $2p_{3/2}$	1021.50	1.67	848568.40		
	Zn $2p_{1/2}$	1044.50	1.67	439533.30		
	χ	23.0				

Γ: Full width at half maximum, LBE: Low binding energy component, IME: Intermediate binding energy component, HBE: High binding energy component, χ is the separation between the energies of the Zn 2p spin orbit split and Δ is the difference in binding energy values between zinc $2P_{3/2}$ and the LBE component of O 1s.

CHAPTER FIVE

ELECTRICAL PROPERTIES

5.1 Electrical properties

This chapter discusses the electrical properties of the films obtained by Van der Pauw technique and Hall measurement system. The three essential parameters that are of interest in electrical analysis of thin films are: (i) resistivity (ρ), (ii) carrier concentration (N), and (iii) mobility (μ). The experimental values obtained are shown in Table 5.1

As seen from the table, the as-deposited films on unheated substrates were highly resistive, with resistivity values that were beyond the detection limit of our system. Consequently, the electrical parameters for these films were not recorded. A similar observation was reported by Hang [46] *et al.* and Yinzhu *et al* [47]. XPS results from the previous chapter revealed that the as-deposited films had a higher stoichiometry than the annealed films. It has been reported that stoichiometric films are highly resistive. Upon annealing at 300 ^{o}C, the resistivity of the films deposited on unheated substrates was reduced to 6.50×10^{4} Ω.cm. Furthermore, annealing at 400 ^{o}C substantially reduced the resistivity to 3.06×10^{-1} Ω.cm, representing five orders of magnitude reduction in resistivity. This clearly shows the role of H_2 annealing temperature on the resistivity of undoped ZnO thin films.

For the films deposited on heated substrates, the as-deposited films exhibited high resistivity beyond the detection limit of our system. However, when the films were annealed at 300 ^{o}C, the resistivity decreased to 6.34×10^{-1} Ω cm. This decrease is five orders of magnitude lower in comparison with the films deposited on unheated substrates and annealed at 300 ^{o}C. This reduction was brought about as a result of substrate heating. Clearly, this shows that increasing the substrate temperature can lead to a significant increase in the conductivity of the films. Further annealing at 400 ^{o}C led to a significant reduction in the resistivity by two orders of magnitude compared to the films annealed at 300 ^{o}C. It is important to stress that the heated substrates exhibited a better conductivity compared with unheated substrates for the same corresponding annealing temperature. The lowest resistivity obtained was 9.00×10^{-3} Ω.cm, for films deposited on heated substrates and annealed at 400 ^{o}C.

The decrease in the resistivity as a result of post growth hydrogen annealing treatment can be explained with the aid of the reduction equation below:

$$ZnO + H_2 \rightarrow Zn_i + e^i + \frac{1}{2}O_{2(g)} \qquad (5.1)$$

where Zn_i and e^i represent generated interstitial zinc and charge carrier, respectively. The interstitial zinc ions thus generated act as donors, which provide the charge carriers, which thus lead to increase in conductivity [48]. Also, it has been reported that the decrease in resistivity could be attributed to an increase in oxygen vacancies which act as donor centers when the films are annealed in reducing environment[8,44]. From chapter four, we saw that more oxygen vacancies were created at 300 and 400 ^{o}C annealing temperatures for the films deposited on unheated substrates. This explains the reduction

in resistivity as a result of increased oxygen vacancies generated following hydrogen annealing.

This explanation is also valid for with the film deposited on heated substrate and annealed at 300 ^{o}C. However, for 400 ^{o}C annealing temperature, the XPS results indicated that the oxygen attached to the zinc oxide crystal increased, implying a decrease in oxygen vacancies. One would expect a corresponding increase in resistivity values for these films following a decrease in oxygen vacancies. On the contrary, a significant decrease in the resistivity was observed, this confirmed the fact that the increase in the LBE component resulted from the significant reduction in the adsorbed oxygen in the films. It is important to note that the reduction in resistivity can also be attributed to increased grain growth and agglomeration that resulted from annealing and substrate temperature.

The resistivity of thin films is strongly related to the carrier concentration and mobility [34]. The carrier concentration increased substantially when the films were annealed at 300 ^{o}C and 400 ^{o}C for both heated and unheated substrates. Generally, undoped zinc oxide exhibits n type conductivity. The origin of the *n* type conductivity has been very controversial. Previously, researchers believed it was related to native defects such as oxygen vacancies and zinc interstitials. However, a recent theory by Van de walle *et al.* [49] suggests that the source of conductivity is related to interstitial hydrogen incorporated during film growth. On this basis, post growth hydrogen annealing is thought to have a profound effect on carrier concentration. As the annealing temperature was raised from 300 to 400 ^{o}C, there was a dramatic increase in the carrier concentration for both substrates (heated and unheated), with the films deposited on the heated

substrates having the highest carrier concentration for any given annealing temperature. This result is consistent with previous work on the effect of substrate temperature on carrier concentration. The increase in carrier concentration in each case indicates the formation of a shallow donor level as a result of hydrogen having been incorporated into the ZnO crystal.

Furthermore, H_2 annealing facilitates the desorption of oxygen in the grain boundaries which act as a trap for the carriers. The negatively charged species (chemisorbed O_2), form depletion regions near the grain boundary surfaces, decreases the free carrier concentration and Hall mobility [34]. However, my results show an increasing trend in the carrier concentration and Hall mobility. This indicates that the depletion regions in the films were removed by passivation of the grain boundary surfaces during post deposition annealing in hydrogen atmosphere. This explanation is confirmed by the XPS results, which show a gradual reduction in the HBE component as the annealing temperature increased. As stated in the previous chapter, the HBE component is related to chemisorption of oxygen, which acts as traps for charge carriers. The complete removal of this component upon annealing justifies the increment in charge carriers concentration and Hall mobility observed in the electrical results.

There was an increase in mobility as the annealing temperature increased for the films deposited on heated and unheated substrates. The increase was more apparent for the films deposited on heated substrates. Ordinarily, this result is unexpected because a profound increase in carrier concentration, as seen from the carrier concentration results, should lead to an increased carrier scattering, which will consequently result into reduction in mobility. However, the mobility of the films deposited on both substrates

increased as the annealing temperature increased. The highest mobility was 15 cm^2/Vs, which correspond to the films deposited on heated substrate and annealed at 400 ^oC. It is important to point out that if the incorporated hydrogen only introduced a shallow donor level, the direct linear relationship between increase in mobility and annealing temperature will not be anticipated. Hence, the observed increase in both mobility and carrier concentration suggest that a substantial fraction of the incorporated hydrogen passivates defects at grain boundaries. Hence, the incorporated hydrogen not only introduces a shallow donor level , but also passivates most of the defect [50]. It is observed that the increase in grain size for both categories of substrates induces improvement of mobility due to the decrease grain boundaries [24].

Table: 5.1 Result of electrical measurements.

Substrates temperature	Annealing temperature (^oC)	Resistivity ρ (Ω cm)	Carrier Concentration N ($1/cm^{-3}$)	Mobility μ ($cm^2/V.s$)
Unheated	As-deposited	Highly Resistive		
Unheated	300	6.50×10^{4}	1.76×10^{18}	5.46
Unheated	400	3.06×10^{-1}	3.17×10^{18}	6.43
400 ^oC	As-deposited	Highly Resistive		
400 ^oC	300	6.34×10^{-1}	3.32×10^{18}	2.97
400 ^oC	400	9.00×10^{-3}	4.61×10^{19}	15.06

In conclusion, the films annealed at 400 ^{o}C and deposited on heated substrate resulted in the highest conductivity, largest carrier concentration and mobility. Hence this condition is the optimum condition to obtain the best result for the conductivity of the films.

CHAPTER SIX

OPTICAL PROPERTIES

6.1 Optical Properties

In this chapter, I discuss the role of H_2 annealing and substrate temperature on the optical properties of ZnO thin films. These properties include the band gap (E_g) and the absorption coefficient (α). Accurate determination of these optical constants is very crucial for optical applications. The value of these optical constants obtained is usually dependent on the preparation conditions and the methods employed in the extraction of the constants from experimental measurements [30, 31].

6.2 Optical transmittance

Figures 6.1 and 6.2 show the transmittance spectra of the films deposited on unheated substrates. All the spectra exhibited sharp absorption near the band-edge of ZnO. This is a clear indication of the high optical quality of the films [50]. The as-deposited films showed a slightly higher optical transmittance compared to the annealed films. This is due to the dependence of the transmittance of the films on the surface morphology [51,52]. The reduction observed in the transmittance spectra of the annealed films may be attributed to light scattering due to increased surface roughness, or absorption due to defects such as oxygen vacancies [53]. The AFM results indicated that the surface roughness of the annealed films was higher than that of the as-deposited films. Consequently, the annealed films showed a relatively lower optical transmittance than the

as- deposited films. The transmittance of the films within the visible range (400-700 nm) approached 90%, making the films ideal for transparent conducting oxide applications. The oscillations in the transmission spectra of the films resulted from the interference in the films due to multiple reflection at the air-ZnO and ZnO-substrate interfaces. Such patterns suggest that the thickness of the films was uniform [6,54].

Films deposited on heated substrates exhibited transmittance spectra that were different from those on unheated substrates, as shown in Figures 6.3 and 6.4. The following deductions can be made from the transmittance spectra of the films deposited on heated substrates.

(i) Films annealed at 400 ^{o}C exhibited a higher transmittance compared to the as-deposited films and the films annealed at 300 ^{o}C. This may be ascribed to the increase in grain size for the films annealed at 400 ^{o}C, as seen from the AFM results. This result is similar to previous work on ZnO films deposited on heated substrates [55].

(ii) The transmittance within the visible range (400-700 nm) reached 95 % for the films deposited on heated films as compared to 90 % for the films deposited on unheated substrates. The increase in the transmittance clearly shows the effect of substrate temperature in improving the average optical transmittance. This effect may result from changes in the microstructure and crystallinity of the films as seen from the XRD results.

A similar result was obtained by Lee et al. [50].

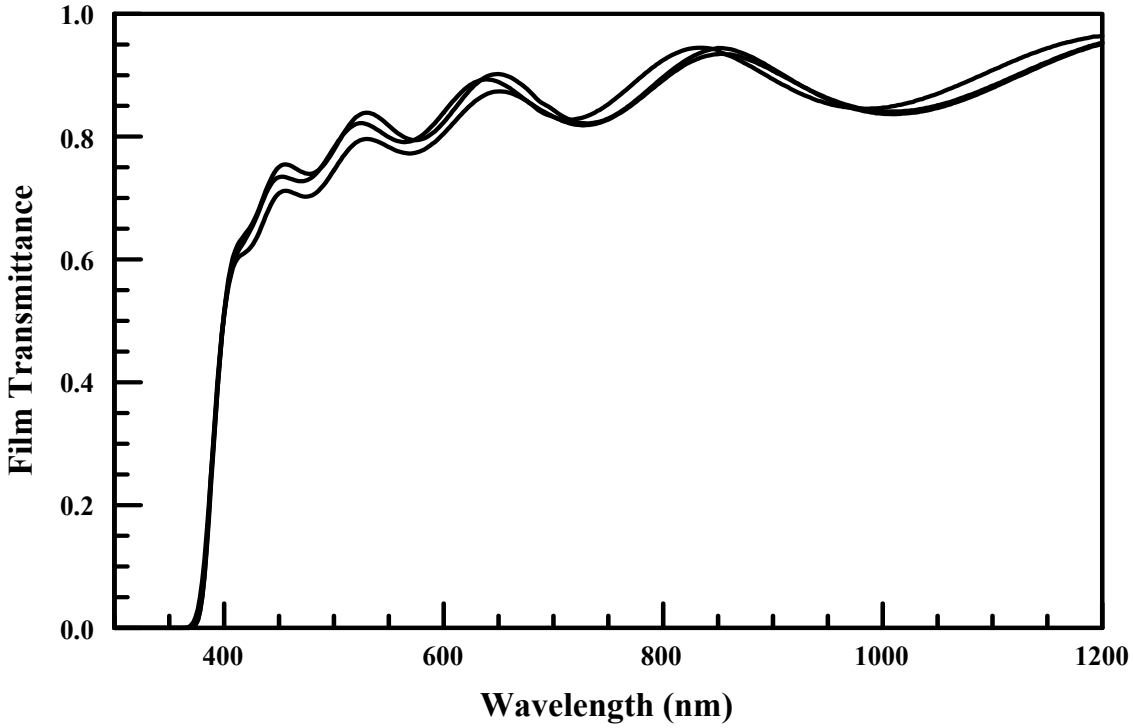

Figure 6.1: Transmittance Spectra for the films deposited on unheated substrate.

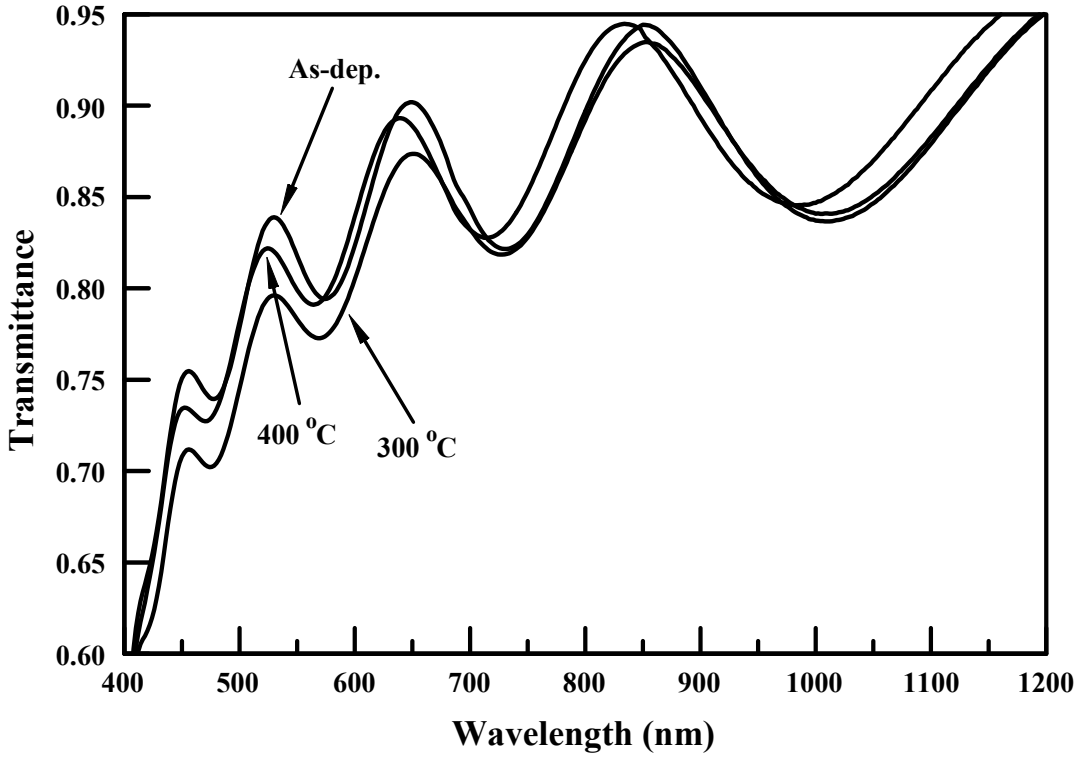

Figure 6.2: Enlarged view of the transmittance spectra of the films deposited on unheated substrate. The annealing temperatures are indicated on the spectra.

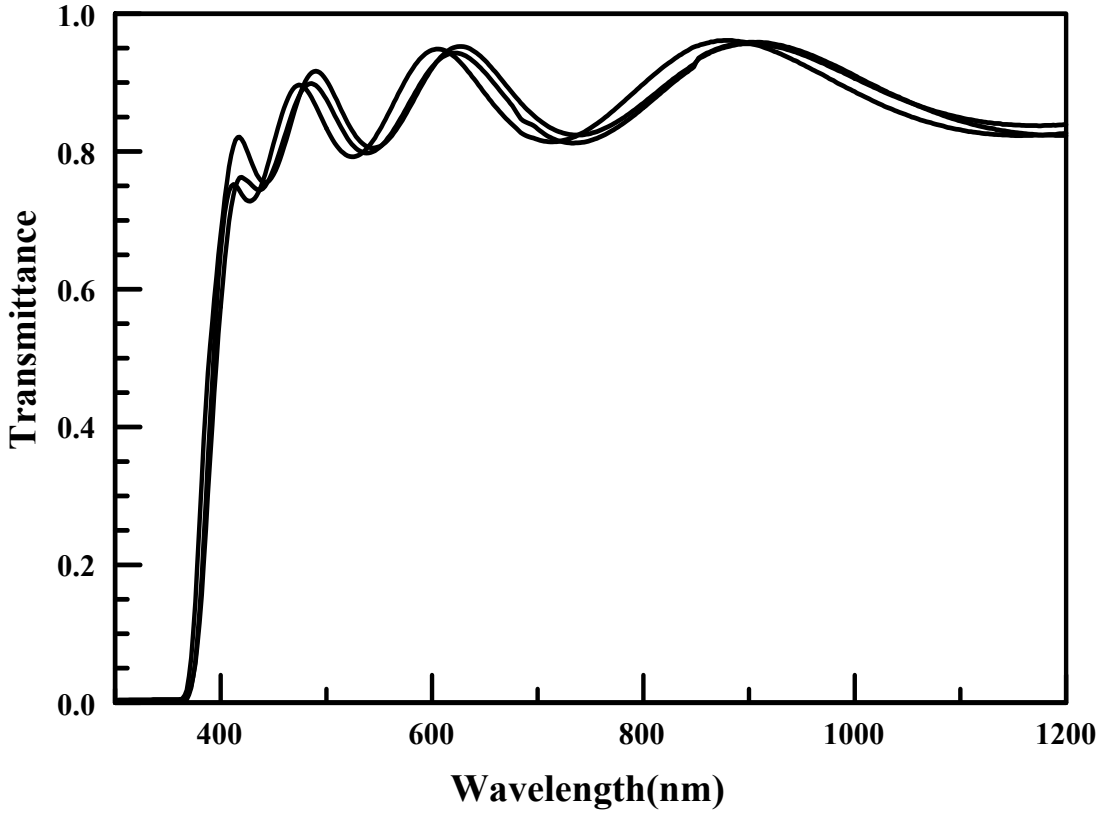

Figure 6.3: Transmittance spectra of the films deposited on heated substrates

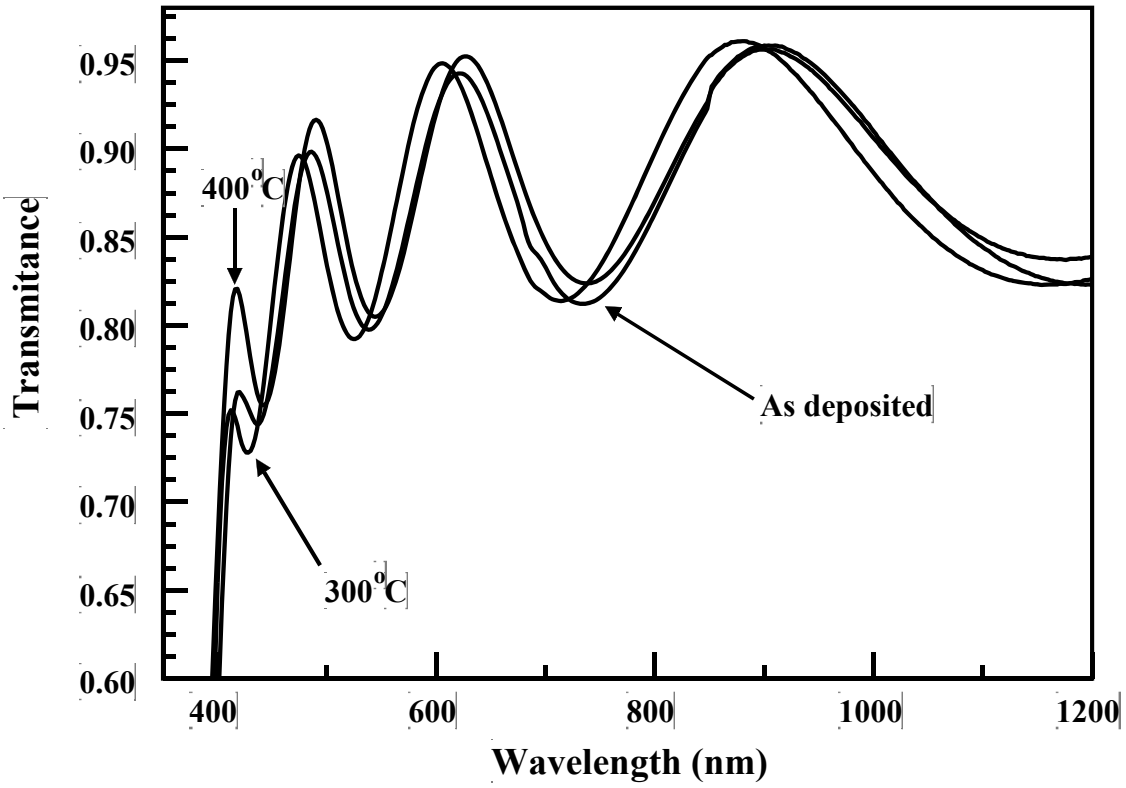

Figure 6.4: Enlarged view of the transmittance spectra of the films deposited on heated substrate. The annealing temperatures are indicated on the spectra.

6.3 Reflectance

Figures 6.5 and 6.6 show the reflectance spectra for the film deposited on unheated and heated substrates, respectively. The reflectance spectra did not reveal further detailed information on the films characteristics. However, they are essential components in the computation of the optical band gap and absorption coefficient of the films.

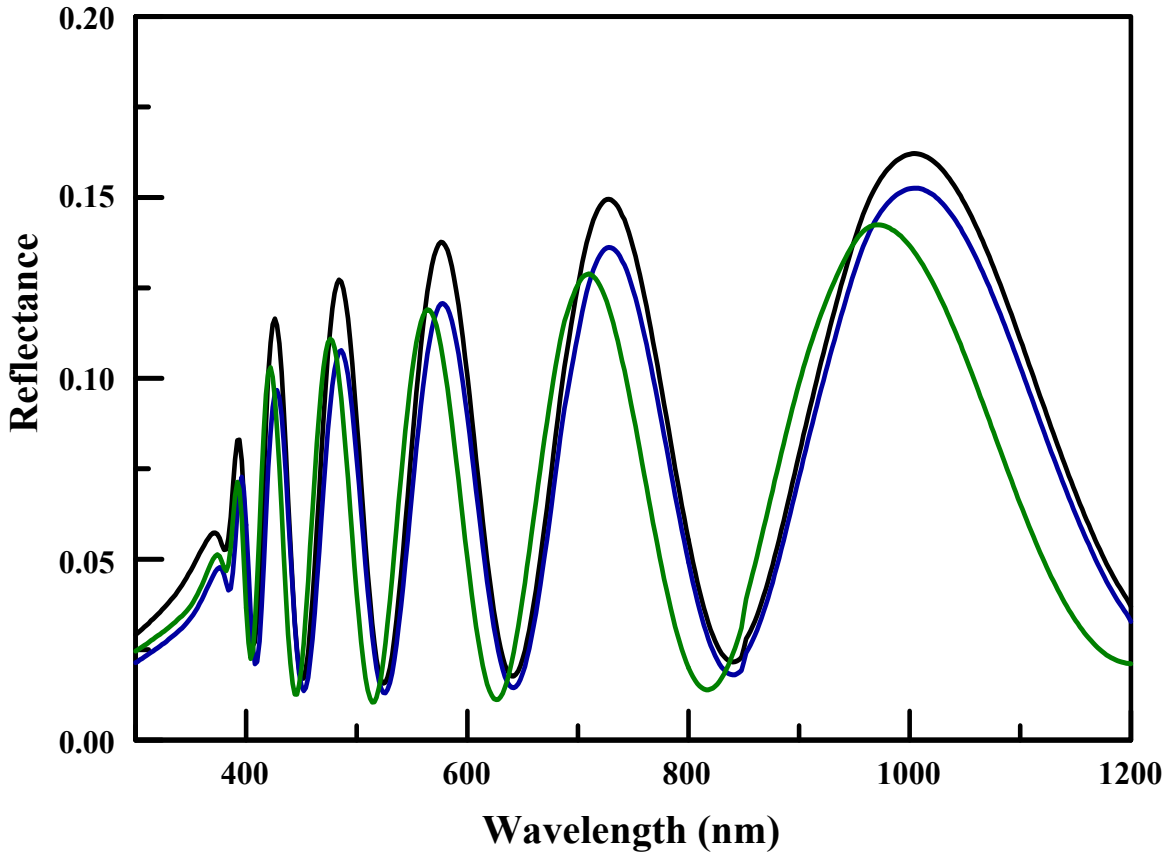

Figure 6.5: Reflectance spectra of the films deposited on unheated substrates.

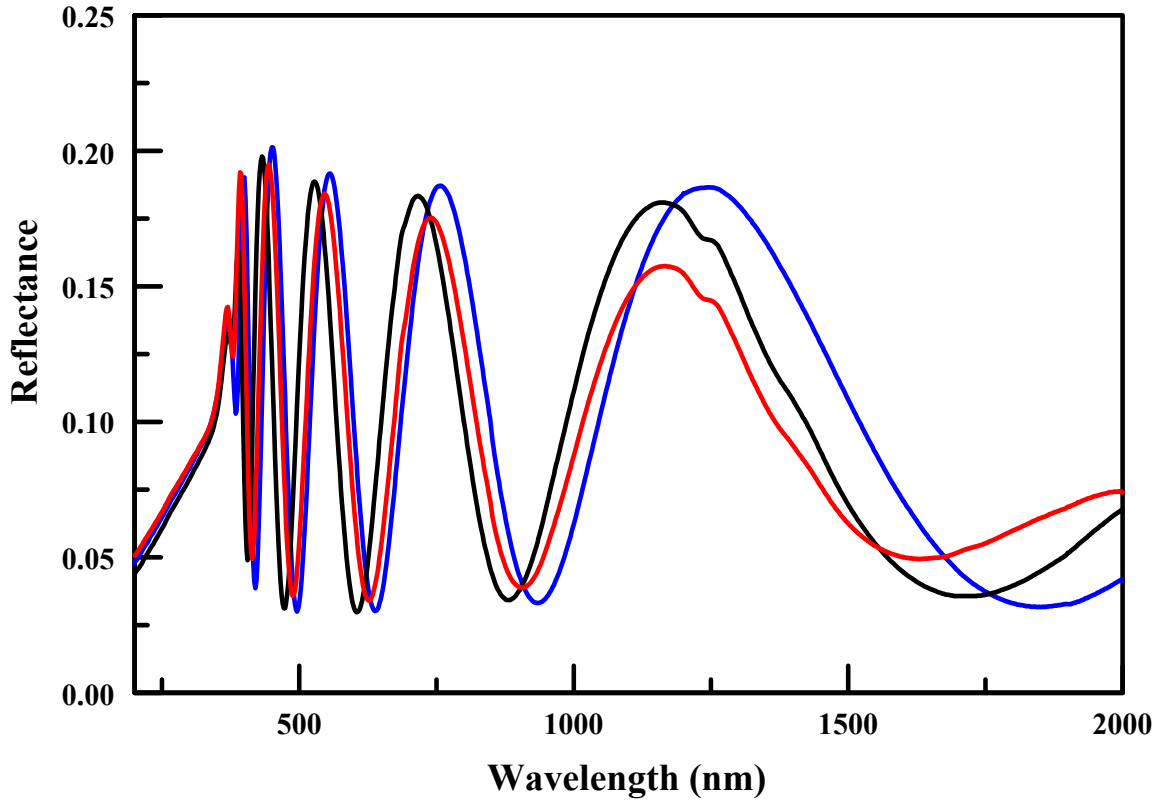

Figure 6.6: Reflectance spectra of the films deposited on heated substrates

6.4 Absorption Coefficient

The transmittance (T) of a thin film can be written as

$$T = \frac{(1-R)^2\, exp\,(-\alpha d)}{1-[R^2 \exp(-2\alpha d)]} \tag{6.1}$$

where R, α and d represent the reflectance, absorption coefficient and thickness of the film, respectively [56]. In the fundamental absorption region, $\alpha > 10^4$ cm^{-1}. Thus the second term in the denominator of equation (6.1) is negligible. Hence, equation (6.1) can be simplified as

$$T = (1-R)^2 e^{(-\alpha d)} \tag{6.2}$$

Rearranging (6.2) , we obtain an expression for the absorption coefficient:

$$\alpha = \frac{1}{d}\, ln \left[\frac{(1-R)^2}{T}\right]. \tag{6.3}$$

Figure 6.7 shows a plot of the absorption coefficient as a function of photon energy (E) for the films deposited on unheated substrates. The effect of H_2 annealing on the absorption coefficient was not apparent until the photon energy reaches a critical value of 3.25 eV. Beyond this value, the effect of annealing as a function of temperature became more pronounced. The rougher the surface of the films, the more the grain boundary density of the films are. This implies higher absorbance (or lower transmittance) [7]. As seen in Fig. 6.7, films that showed the lowest absorption characteristics had also the lowest roughness. While the film annealed at 300 ^{o}C exhibited the most pronounced

absorption characteristics, it is expected that this film will have the highest roughness value. This prediction is consistent with the results obtained from the AFM analysis.

A contrary result was obtained for the films deposited on heated substrates. Figure 6.8 shows the plot of absorption coefficient as a function of photon energy for the films deposited on heated substrates. It was observed that the behavior of absorption characteristics could not be explained merely by considering only the surface roughness. The as-deposited films had the lowest roughness, yet the highest absorption coefficient. Also, the films annealed at 400 ^{o}C had a relatively higher roughness compared with those annealed films at 300 ^{o}C and the as-deposited films. Yet, it had the lowest absorption coefficient. This suggests that substrate temperature played an opposing role to annealing for heated substrates. I suggest that these changes are related to changes in microstructure and crystallinity of the films deposited on heated substrates.

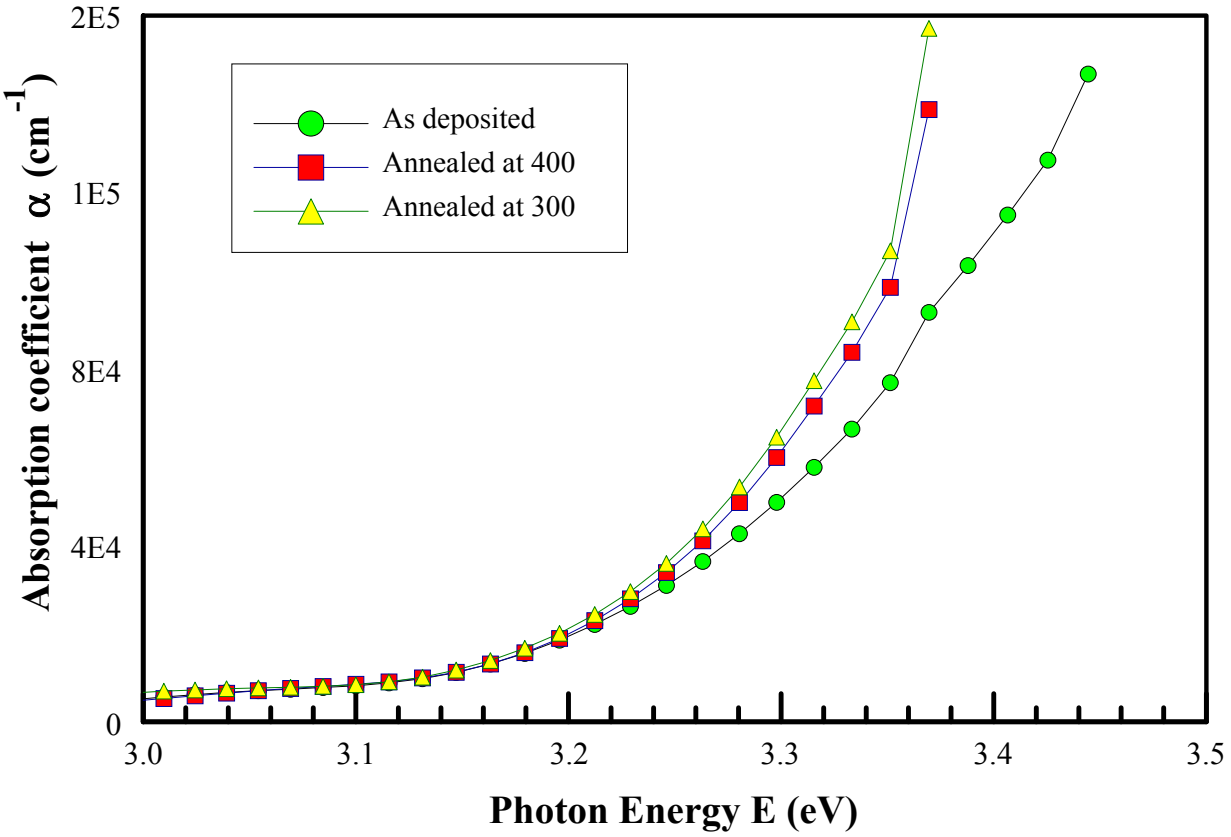

Figure 6.7: Absorption coefficients for the films deposited on unheated substrates.

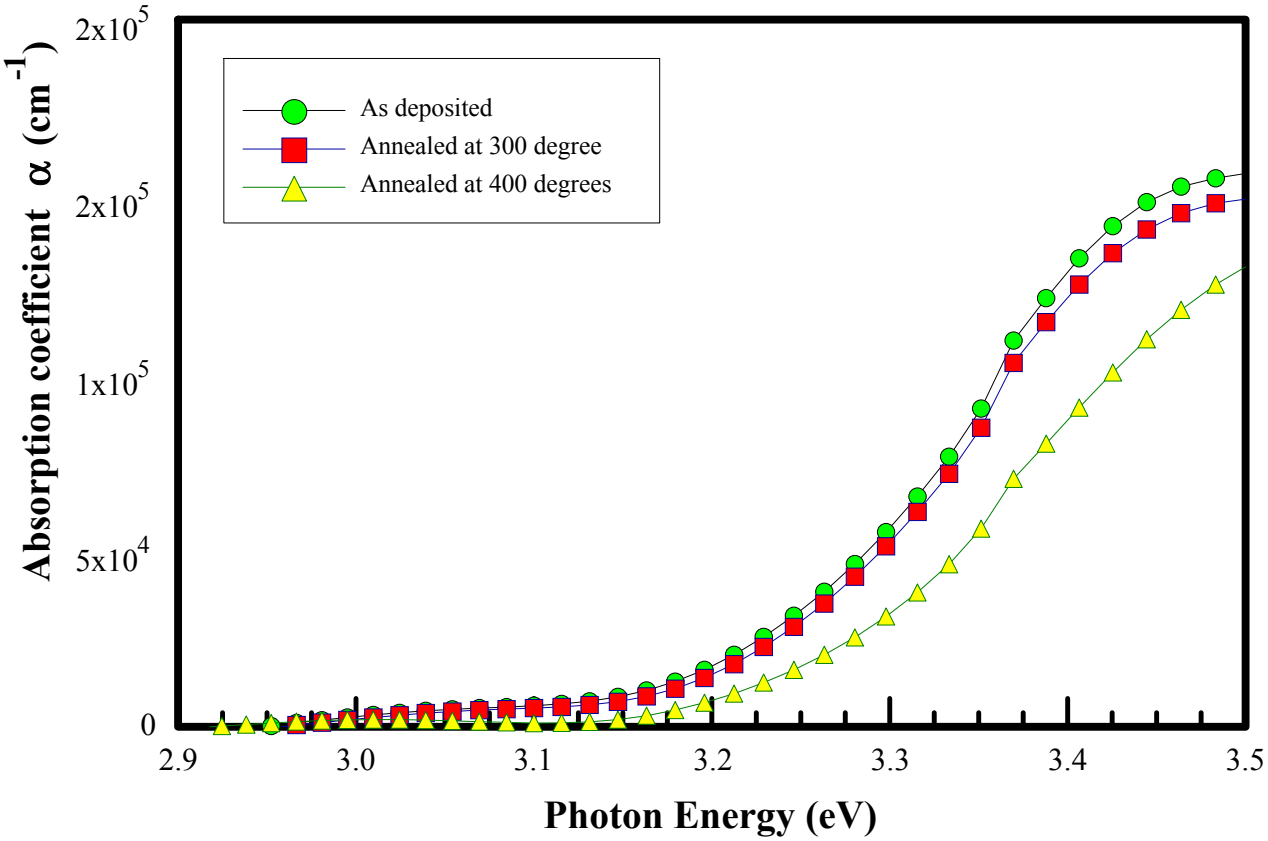

Figure 6.8: Absorption coefficients for the films deposited on heated substrates.

6.5 Band Gap

The relationship between the absorption coefficient and the optical band gap (E_g) is given by

$$\alpha = \frac{\alpha o}{E} \ (E\text{-}E_g)^{\eta} \qquad (6.4)$$

where α_o is a constant with values between 10^5-10^6 cm^{-1}. The constant η depends on the types of electronic transitions involved. For a direct band gap semiconductor, the value of the constant η is $1/2$ which corresponds to direct allowed transitions [12]. Zinc oxide is a direct band gap material. Hence, equation (6.4) takes the form below.

$$\alpha = \frac{\alpha o}{E} \ (E\text{-}E_g)^{1/2} \qquad (6.5)$$

In order to calculate the band gap, the quantity $(\alpha E)^2$ was plotted as a function of photon energy. The linear region of the curve was fitted using linear regression analysis, and the line extrapolated to the intercept with the horizontal axis (where αE =0). Such plots are referred to as Tauc plots [23]. Figures 6.8 and 6.9 give representative Tauc plots for films deposited on unheated and heated substrates, respectively. The resulting band gap values are giving in Table 6.1

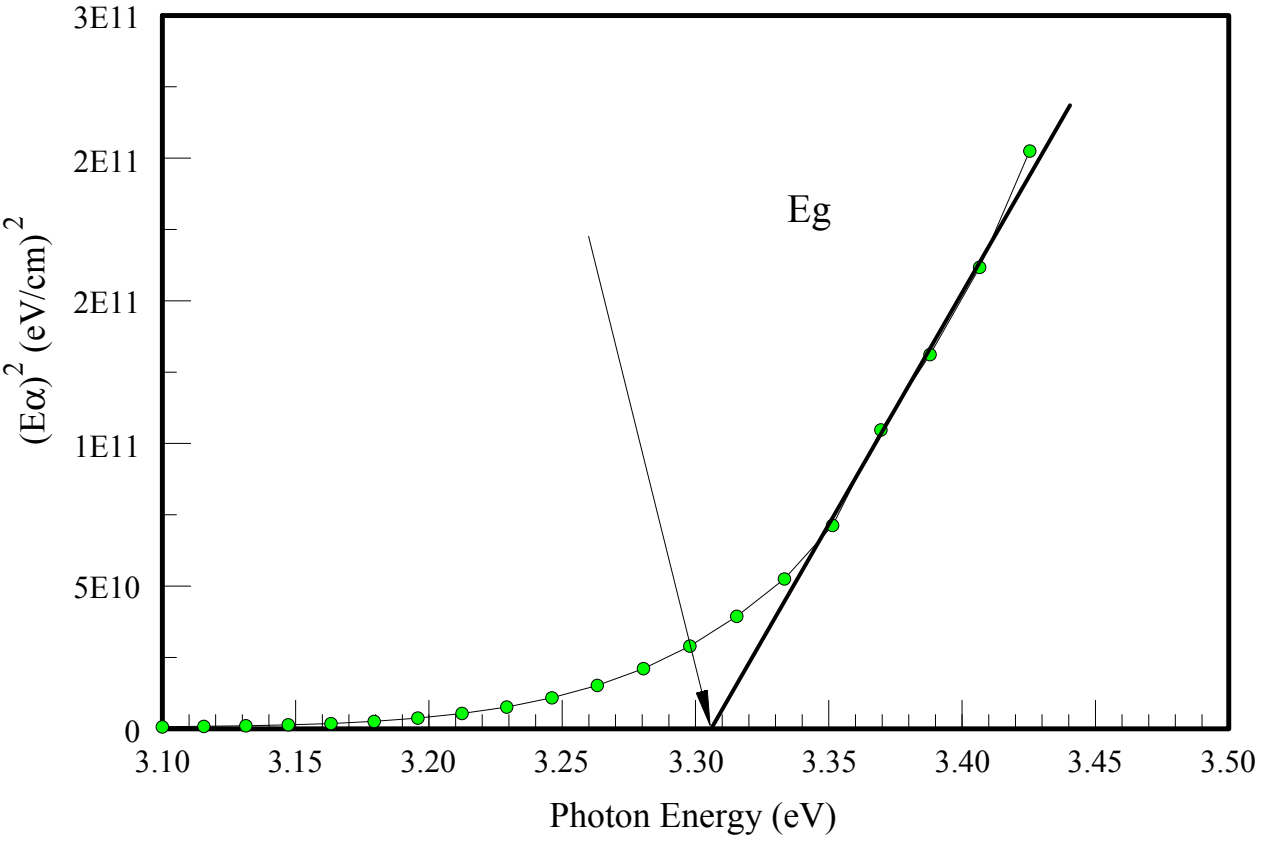

Figure 6.9: A representative Tauc plot for as-deposited films grown on unheated substrate

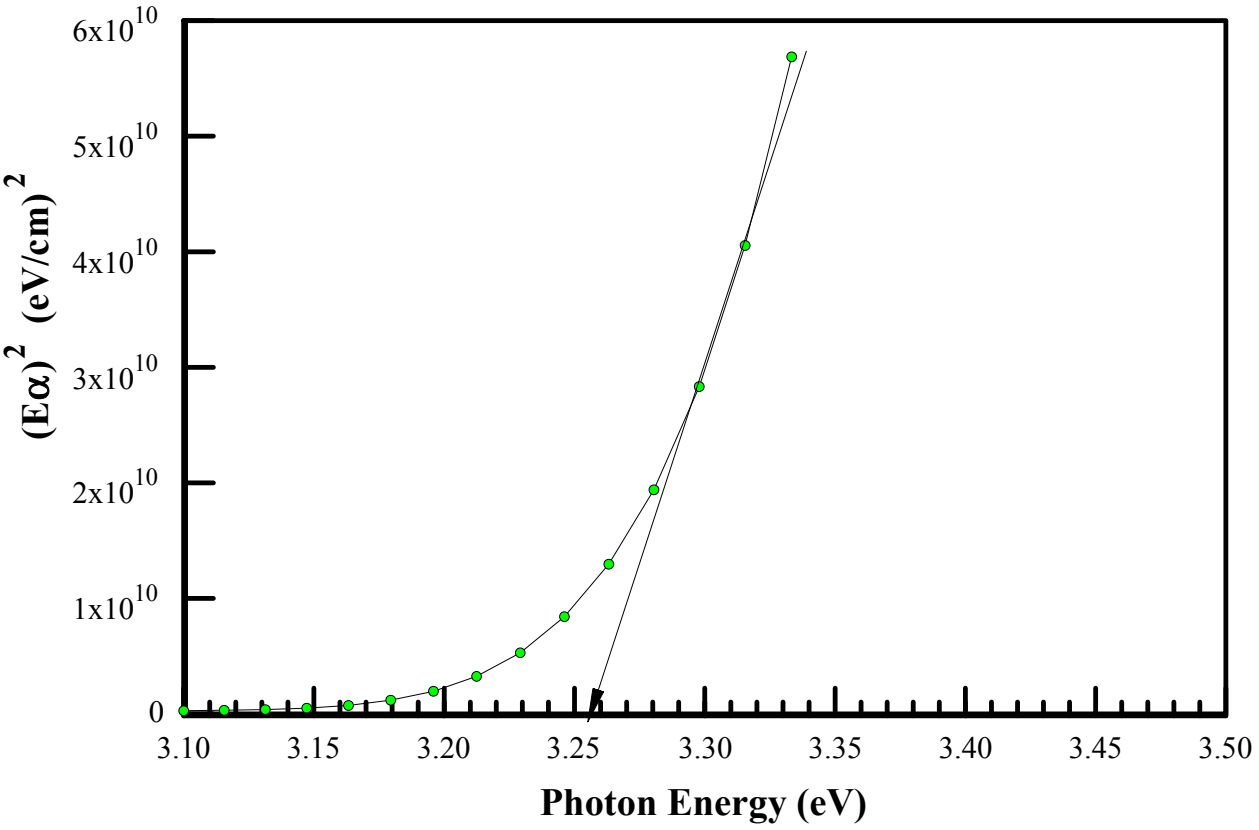

Figure 6.10: A representative Tauc plot for as-deposited films grown on heated substrate

As seen from Table 6.1, the band gap increased slightly upon annealing for the films deposited on heated substrates. It was suggested that the increase in optical bandgap results from oxygen vacancies generated as a result of annealing in a reducing medium. Furthermore, it was reported that an increment in defects would lead widening of the optical band gap [57].

The slight increase in the band gap for the films deposited on heated substrates can be explained using Burstein-Moss (BM) effect. This means that the Fermi level was raised into the conduction band of the degenerate semiconductor upon annealing in hydrogen,

which is responsible for the blue shift observed in the transmission spectra shown in Fig 6.10 [44,58].

However, a contrary result was observed for the films deposited on unheated substrates, which exhibited a slight decrease in optical band gap as the annealing temperature was increased. The decease of the optical band gap caused the shift of the Fermi level towards lower energy and this can be viewed as a reverse of the BM effect [53]. A similar decrease was reported in the literature [10]. It is noteworthy that the band gap value for the as-deposited films was 3.31 eV. The result is in agreement with previous studies [12,32]. In summary , the annealing had a less pronounced effect on the optical band gap energy of the films. A similar result was reported by Hyeong *et al.* [11].

Table 6.1: calculated values of direct band gaps

Substrate Temperature	As- deposited	Annealing Temperature ^{o}C	
		300 ^{o}C	400 ^{o}C
	E_g (eV)	E_g (eV)	E_g (eV)
Unheated	3.31	3.25	3.23
400 ^{o}C	3.24	3.25	3.28

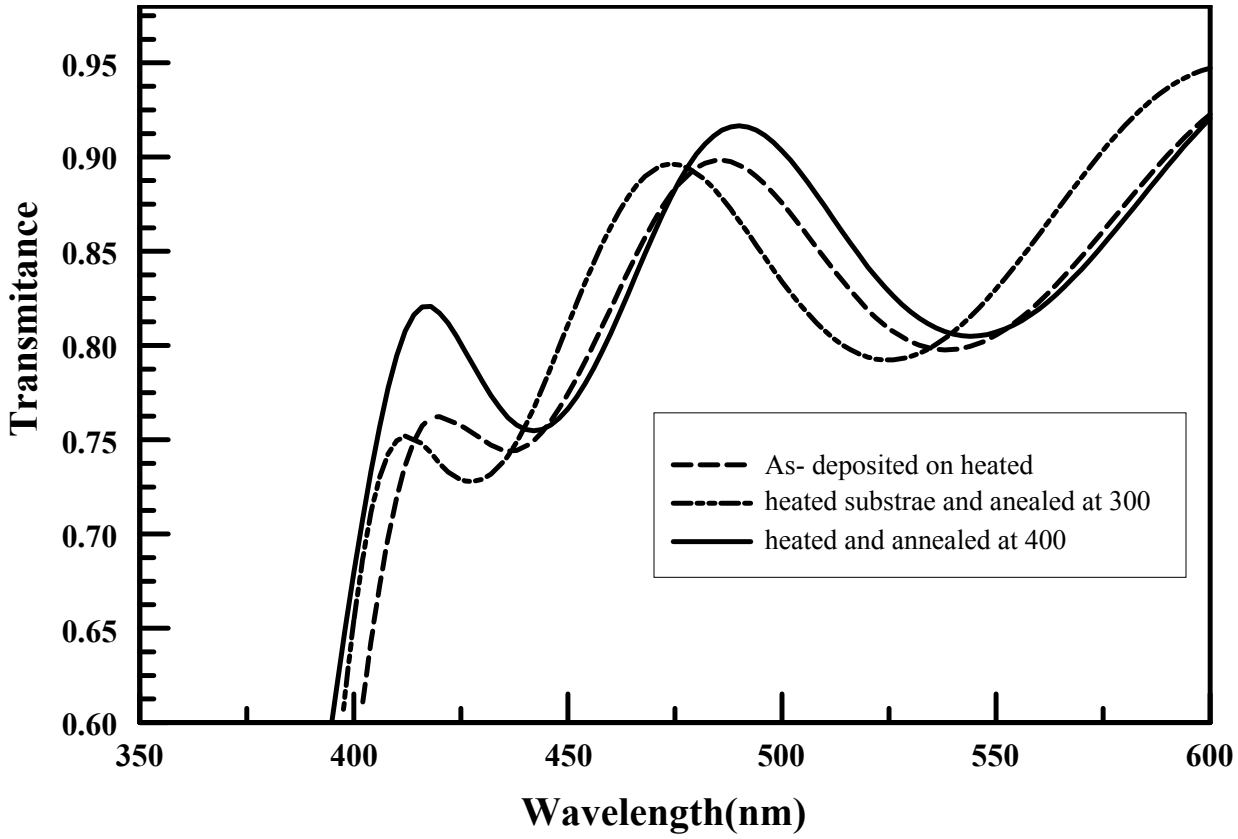

Figure 6.11: Illustration of Burstein –Moss effect for the films deposited on heated substrates.

CHAPTER SEVEN

CONCLUSION

From the foregoing chapters, the following conclusions can be made:

(i) The films were all polycrystalline with (002) and (100) preferred orientations for unheated and heated substrate, respectively. Substrate heating was responsible for switching of the preferred direction from the well-known (002) to (100) plane.

(ii) It was observed that increasing the annealing temperature led to an increase in crystallite size for both unheated and heated substrates,. The crystallite size was enhanced for films deposited on heated substrates.

(iii) Similarly, the lateral grain size also depends on annealing temperature. It increased as the annealing temperature increased. However, there was a reduction in the grain size for the films deposited on unheated substrates and annealed at 300 ^{o}C.

(iv) Oxygen vacancies increased as the annealing temperature increased for the as deposited films in both categories of substrates, except for the film deposited on heated substrates and annealed at 400 ^{o}C. This clearly shows that besides oxygen vacancies, changes in microstructure of the films could also be responsible for reduction in resistivity.

(v) The resistivity of ZnO is reduced when the films are subjected to post growth hydrogen annealing.

(vi) Substrate temperature played a significant role in the reduction of resistivity of ZnO thin films.

(vii) The optimum conductivity was obtained when the films were deposited on heated substrates and annealed at 400 ^{o}C. Further increase in the annealing temperature led to etching of the films.

(viii) The as-deposited films in for unheated and heated substrate were very transparent in the visible range, with optimum transparency reaching approximately 80-90%. For the films deposited on unheated substrates, annealing led to slight reduction in the transparency. For the films deposited on heated substrate, annealing enhanced the transparency of the films.

(ix) Annealing and substrate heating did have effects on the optical properties of the films

REFERENCES

[1] U. Ilyas, R. S. Rawat, T. L. Tan, P. Lee, R. Chen, H. D. Sun, and L. Fengji, "Oxygen rich p -type ZnO thin films using wet chemical route with enhanced carrier concentration by temperature-dependent tuning of acceptor defects," Journal of Applied Physics 110 093522 (2011) vol. 093522, pp. 1–7, 2011.

[2] M. K. Puchert, P. Y. Timbrell, and R. N. Lamb, "Postdeposition annealing of radio frequency magnetron sputtered ZnO films," Journal Vaccum Technol.vol. 14, no. 4, pp. 2220–2230, 1996.

[3] Online resources: http://www.zinc.org/info/zinc_oxide_applications.

[4] D. Snigurenko, R. Jakiela, E. Guziewicz, E. Przezdziecka, M. Stachowicz, K. Kopalko, A. Barcz, W. Lisowski, J. W. Sobczak, M. Krawczyk, and A. Jablonski, "XPS study of arsenic doped ZnO grown by Atomic Layer Deposition," Journal Alloys Compound, vol. 582, pp. 594–597, 2014.

[5] B. Singh, Z. A. Khan, I. Khan, and S. Ghosh, "Highly conducting zinc oxide thin films achieved without postgrowth annealing Highly conducting zinc oxide thin films achieved without postgrowth," Applied Physics Letter 97 vol. 241903, no. 2010, pp. 2012–2015, 2014.

[6] O. Lupan and T. Pauporte, "Effects of annealing on properties of ZnO thin films prepared by electrochemical deposition in chloride medium," Applied Surface Science vol. 256, pp. 1895–1907, 2010.

[7] C. Y. Ã. Zhang, "The influence of post-growth annealing on optical and electrical properties of p-type ZnO films," Material Science in Semiconctor Processing. vol. 10, pp. 215–221, 2007.

[8] E. Çetinörgü, S. Goldsmith, and R. L. Boxman, "The effect of substrate temperature on filtered vacuum arc deposited zinc oxide and tin oxide thin films," Journal Crystal Growth, vol. 299, no. 2, pp. 259–267, Feb. 2007.

[9] J. Lee and B. Park, "Characteristics of Al-doped ZnO thin films obtained by ultrasonic spray pyrolysis : effects of Al doping and an annealing treatment," Material Science and Engineering vol. B 106, pp. 242–245, 2004.

[10] B. L. Zhu, J. Wang, S. J. Zhu, J. Wu, R. Wu, D. W. Zeng, and C. S. Xie, "Infl uence of hydrogen introduction on structure and properties of ZnO thin fi lms during sputtering and post-annealing," Thin solid films vol. 519, pp. 3809–3815, 2011.

[11] J. Lee, “Effects of hydrogen incorporation and heat treatment on the properties of ZnO : Al films deposited on polymer substrate for flexible solar cell applications,” Current Applied Physics, vol. 10, no. 3, pp. S515–S519, 2010.

[12] Q. Yu, H. Yang, W. Fu, L. Chang, J. Xu, C. Yu, R. Wei, K. Du, H. Zhu, M. Li, and G. Zou, “Transparent conducting yttrium-doped ZnO thin films deposited by sol – gel method,” Thin solid films vol. 515, pp. 3840–3843, 2007.

[13] S. Lee, D. Cheon, W. Kim, M. Ham, and W. Lee, “Applied Surface Science Ga-doped ZnO films deposited with varying sputtering powers and substrate temperatures by pulsed DC magnetron sputtering and their property improvement potentials,” Applied Surface Science, vol. 258, no. 17, pp. 6537–6544, 2012.

[14] Ü. Özgür, Y. I. Alivov, C. Liu, A. Teke, M. A. Reshchikov, S. Do, and V. Avrutin, “Applied Physics Reviews: A comprehensive review of ZnO materials and devices,” pp. 1–103, 2005.

[15] D. A. Neamen, Semiconductor Physics and Devices: Basic Principles,. 2008.

[16] Wikepidia, “http://en.wikipedia.org/wiki/Crystallographic_defect,” online Mater.

[17] M. D. Mccluskey and S. J. Jokela, “Applied Physics Reviews — Focused Review Defects in ZnO,” pp. 1–13, 2009.

[18] J. F. Chang, W. C. Lin, and M. H. Hon, “Effects of post-annealing on the structure and properties of Al-doped zinc oxide thin films,” Applied Surface Science Vol. 183, pp. 18–25, 2001.

[19] K. Yim and Æ. C. Lee, “Dependence of the electrical and optical properties of sputter-deposited ZnO : Ga films on the annealing temperature , time , and atmosphere,” Journal Material Science : Mater Electron. pp. 385–390, 2007.

[20] H. Chang, F. Wang, J. Chao, C. Huang, and H. Liu, “Effects of thickness and annealing on the properties of Ti-doped ZnO fi lms by radio frequency magnetron sputtering,” Current Applied Physics, vol. 11, no. 1, pp. S185–S190, 2011.

[21] C. Charpentier, P. Prod, and P. Roca, “Microstructural , optical and electrical properties of annealed ZnO : Al thin fi lms,” Thin Solid Films, vol. 531, pp. 424–429, 2013.

[22] J. Kim, M. Kim, J. Yu, and K. Park, “H 2 / Ar and vacuum annealing effect of ZnO thin films deposited by RF magnetron sputtering system,” Current Applied Physics, vol. 10, no. 3, pp. S495–S498, 2010.

[23] Huang, Changgang, Deng, Zhonghua "Effects of hydrogen annealing on the structural , optical and electrical properties of indium-doped zinc oxide films" Journal of Material Science: Mater Electron (2010).

[24] H. Park, K. Chung, and J. Park, "A role of oxygen vacancy on annealed ZnO fi lm in the hydrogen atmosphere," Current Applied Physics, vol. 12, pp. S164–S167, 2012.

[25] Online Material for Sputtering: Http://www.semicore.com/what-is-sputtering,

[26] Online Material for XRD: Http://web.pdx.edu/~pmoeck/phy381/Topic5a-XRD.pdf,." .

[27] http://serc.carleton.edu/research_education/geochemsheets/BraggsLaw.html, "

[28] Online Material for AFM:,*http://en.wikipedia.org/wiki/Atomic_force_microscopy*.

[29] "AFM IMAGE." Http://en.wikipedia.org/wiki/Atomic_force_microscopy,

[30] Van der Pauw Technique. Http://electron.mit.edu/~gsteele/vanderpauw/, "." .

[31] Course Material at Caltech USA." .Http://mmrc.caltech.edu/SS_XPS/XPS_PPT/XPS_Slides.pd, "

[32] W. W. Liu, B. Yao, Y. F. Li, B. H. Li, Z. Z. Zhang, C. X. Shan, D. X. Zhao, J. Y. Zhang, D. Z. Shen, and X. W. Fan, "Structure , luminescence and electrical properties of ZnO thin films annealed in H 2 and H 2 O ambient : A comparative study," Thin Solid Films, vol. 518, no. 14, pp. 3923–3928, 2010.

[33] M. Lee, J. Lim, J. Bang, W. Lee, and J. Myoung, "Effect of the thickness and hydrogen treatment on the properties of Ga-doped ZnO transparent conductive films," Applied Surface Science .vol. 255, pp. 3195–3200, 2008.

[34] B. Oh, M. Jeong, D. Kim, W. Lee, and J. M. Ã, "Post-annealing of Al-doped ZnO films in hydrogen atmosphere," Journal of Crystal Growth .vol. 281, pp. 475–480, 2005.

[35] P. Banerjee, W.-J. Lee, K.-R. Bae, S. B. Lee, and G. W. Rubloff, "Structural, electrical, and optical properties of atomic layer deposition Al-doped ZnO films," Journal Applied Physics, vol. 108, no. 4, p. 043504, 2010.

[36] J.-W. Kim, H.-B. Kim, and D.-K. Kim, "Effect of RF power on an Al-doped ZnO thin film deposited by RF magnetron sputtering," Journal of the Korean Physical Society 2011.

[37] S. Yoon, I. Huh, J. Lim, and B. Yoo, "Annealing effects on electrical and optical properties of ZnO thin films synthesized by the electrochemical method," Current Applied Physics, vol. 12, no. 3, pp. 784–788, 2012.

[38] W. Liu, B. Yao, Y. Li, B. Li, C. Zheng, and B. Zhang, "Annealing temperature dependent electrical and optical properties of ZnO and MgZnO films in hydrogen ambient," Applied Surface Science . vol. 255, pp. 6745–6749, 2009.

[39] T. Sasabayashi , N. Ito, E. Nishimura , P.K. Song,"Comparative study on structure and internal stress in tin-doped indium oxide and indium-zinc oxide films deposited by r.f. magnetron sputtering" Thin Solid Films 445 (2003) 219–223

[40] M. F. Al-Kuhaili, S. M. A. Durrani, I. A. Bakhtiari, and M. Saleem, "Optical constants of vacuum annealed radio frequency (RF) magnetron sputtered zinc oxide thin films," Optics Communication, vol. 285, no. 21–22, pp. 4405–4412, Oct. 2012.

[41] M. K. Ryu, S. H. Lee, and M. S. Jang, "Postgrowth annealing effect on structural and optical properties of ZnO films grown on GaAs substrates by the radio frequency magnetron sputtering technique," Journal of Applied Physics vol. 92, no. 1, pp. 154–158, 2002.

[42] P. Yao, S. Hang, and M. Wu, "Growth characteristics and properties of Al-doped ZnO thin films by DC magnetron sputtering from AZOY(R) target," Transactions of the Canadian Society for Mechanical Engineering ,vol. 37, no. 3, 2012.

[43] G. Machado, D. N. Guerra, D. Leinen, J. R. Ramos-Barrado, R. E. Marotti, and E. a. Dalchiele, "Indium doped zinc oxide thin films obtained by electrodeposition," Thin Solid Films, vol. 490, no. 2, pp. 124–131, Nov. 2005.

[44] R. Al-gaashani, S. Radiman, A. R. Daud, N. Tabet, and Y. Al-douri, "XPS and optical studies of different morphologies of ZnO nanostructures prepared by microwave methods," Ceramics International, pp. 1–10, 2012.

[45] M. Chen, X. Wang, Y. . Yu, Z. . Pei, X. . Bai, C. Sun, R. . Huang, and L. . Wen, "X-ray photoelectron spectroscopy and auger electron spectroscopy studies of Al-doped ZnO films," Applied Surface Science. vol. 158, no. 1–2, pp. 134–140, May 2000.

[46] K. Lee, N. Cho, E. Yun, and H. G. Nam, "Applied Surface Science Characterization of ZnO thin films grown on various substrates by RF magnetron sputtering," Applied Surface Science. vol. 256, no. 13, pp. 4241–4245, 2010.

[47] Y. Zhang, J. Lu, L. Chen, and Z. Ye, "Properties of N-doped ZnO thin films in annealing process," Solid State Communications. vol. 143, pp. 562–565, 2007.

[48] J. Huang and C. Liu, “The influence of magnesium and hydrogen introduction in sputtered zinc oxide thin films,” Thin Solid Films. vol. 498, pp. 152–157, 2006.

[49] C. G. Van De Walle, “Hydrogen as a Cause of Doping in Zinc Oxide,” Physical Review Letters. vol. 85, no. 1, pp. 0–3, 2000.

[50] P. F. Cai, J. B. You, X. W. Zhang, J. J. Dong, X. L. Yang, Z. G. Yin, and N. F. Chen, “Enhancement of conductivity and transmittance of ZnO films by post hydrogen plasma treatment*,”* Journal of Applied Physics 105. pp. 1–6, 2009.

[51] Y. B. Zhang, G. K. L. Goh, K. F. Ooi, and S. Tripathy, “Hydrogen-related n -type conductivity in hydrothermally grown epitaxial ZnO films,” Journals of Applied Physics 108, 083716 pp. 8–11, 2010.

[52] W. Yang, Z. Wu, Z. Liu, A. Pang, Y. Tu, and Z. Chuan, “Room temperature deposition of Al-doped ZnO films on quartz substrates by radio-frequency magnetron sputtering and effects of thermal annealing,” Thin Solid Films vol. 519, pp. 31–36, 2010.

[53] H. Kim, S. Zh, and M. Kim, “Phys. Status solidi B 248,” vol. 1707, no. 7, pp. 1702–1707, 2011.

[54] J.-P. Lin and J.-M. Wu, “The effect of annealing processes on electronic properties of sol-gel derived Al-doped ZnO films,” Applied Physics Letter, vol. 92, no. 13, p. 134103, 2008.

[55] C. Huang, M. Wang, and Z. Deng, “Effects of hydrogen annealing on the structural , optical and electrical properties of indium-doped zinc oxide films,”Journal Material Science : Mater Electron (2010). pp. 1221–1227, 2010.

[56] M.F Al- Kuhaili, M. Mekki, S.M.A Durrani, I.A Bakhtiari, M.A Dastageer, “Influence of hydrogen annealing on the properties of hafnium oxide thin films,” Journal : Materials Chemstry and Physics. 126(2011) 515-523, 2011.

[57] Y. Natsume and H. Sakata, “Electrical conductivity and optical properties of ZnO films annealed in hydrogen atmosphere after chemical vapor deposition,” Journal of Material Science: Material in Electronics: vol. 2, pp. 87–92, 2001.

[58] C. Eun, P. Moon, S. Kim, J. Myoung, H. Woo, J. Bang, and I. Yun, “Effect of carrier concentration on optical bandgap shift in ZnO : Ga thin films,” Thin Solid Films, vol. 518, no. 22, pp. 6304–6307, 2010.

Vitae

Name	Alade Ibrahim Olanrewaju
Nationality	Nigerian
Date of Birth	14th March, 1983
Email	:talkwithlanre2000@yahoo.com
Address	: Residence on campus, building 5, Room 805.
Academic Background	: B.Sc Applied physics, UNILAG, Nigeria.
	2003-2008
	HND, Industrial Maint Eng,YABATECH. NIG.
	2002-2007

Publication: M. F AL-Kuhaili, **I.O Alade**, and S.M.A Durrani." Optical constants of hydrogenated zinc oxide thin films" optical materials Express, Vol.4, Issue 11, pp. 2323-2332(2014)